Article

Accumulation of the Auxin Precursor Indole-3-Acetamide Curtails Growth through the Repression of Cell Proliferation and Development-Related Transcriptional Networks

Beatriz Sánchez-Parra [1,2], Marta-Marina Pérez-Alonso [2,3], Paloma Ortiz-García [2], José Moya-Cuevas [2], Mathias Hentrich [4] and Stephan Pollmann [2,5,*]

[1] Max-Planck-Institut für Chemie, 55128 Mainz, Germany; B.SanchezParra@mpic.de
[2] Centro de Biotecnología y Genómica de Plantas, Universidad Politécnica de Madrid (UPM) – Instituto Nacional de Investigación y Tecnología Agraria Y Alimentación (INIA), Campus de Montegancedo, 28223 Pozuelo de Alarcón (Madrid), Spain; p.ortiz@upm.es (P.O.G.); jose.moya@upm.es (J.M.C.)
[3] Umeå Plant Science Center, Umeå University, 90736 Umeå, Sweden; marta.perez.alonso@slu.se
[4] Lehrstuhl für Pflanzenphysiologie, Ruhr-Universität Bochum, 44780 Bochum, Germany; mathias.hentrich@rub.de
[5] Departamento de Biotecnología-Biología Vegetal, Escuela Técnica Superior de Ingeniería Agronómica, Alimentaria y de Biosistemas, Universidad Politécnica de Madrid (UPM), 28040 Madrid, Spain
* Correspondence: stephan.pollmann@upm.es; Tel.: +34-910679183

Abstract: The major auxin, indole-3-acetic acid (IAA), is associated with a plethora of growth and developmental processes including embryo development, expansion growth, cambial activity, and the induction of lateral root growth. Accumulation of the auxin precursor indole-3-acetamide (IAM) induces stress related processes by stimulating abscisic acid (ABA) biosynthesis. How IAM signaling is controlled is, at present, unclear. Here, we characterize an *ami1/rooty* double mutant, that we initially generated to study the metabolic and phenotypic consequences of a genetic blockade of the indole glucosinolate and IAM pathways in *Arabidopsis thaliana*. Our mass spectrometric analyses of the mutant revealed that the combination of the two mutations is not sufficient to fully prevent the conversion of IAM to IAA. The detected strong accumulation of IAM was, however, recognized to substantially impair seed development. We further show by genome-wide expression studies that the double mutant is broadly affected in its translational capacity, and that a small number of cell proliferation and plant growth regulating transcriptional circuits are repressed by the high IAM content in the seed. In accordance with the previously described growth reduction in response to elevated IAM levels, our data support the hypothesis that IAM is a growth repressing counterpart to IAA.

Keywords: *Arabidopsis thaliana*, indole-3-acetic acid, indole-3-acetamide, indole glucosinolate, seed maturation, seed size, cell proliferation, plant growth

1. Introduction

The auxin indole-3-acetic acid (IAA) is a major endogenous growth factor in plants and linked with a great variety of different developmental processes and adaptive responses, including elongation growth, polar development, cambial activity, gravitropism and phototropism, respectively. Thus, it is not surprising that IAA is recognized as an essential phytohormone necessary to ensure optimal plant growth and development [1,2]. The main source of auxin in plants is the indole-3-pyruvate (IPyA) pathway, encompassing tryptophan aminotransferases (TAA1/TAR2) and

flavin containing monooxygenases (YUC1-11) that convert L-Trp to IAA via the intermediate IPyA [3,4]. The spatio-temporal expression of these key players in auxin biosynthesis is tightly developmentally controlled [5]. Alongside the main IPyA pathway, plants are assumed to involve a small number of additional pathways in the formation of IAA. These pathways act either redundantly or in a parallel manner with the main route [6-8]. The Brassicaceae family, including the model plant *Arabidopsis thaliana*, possesses the additional indole-3-acetaldoxime (IAOx) pathway (Figure 1).
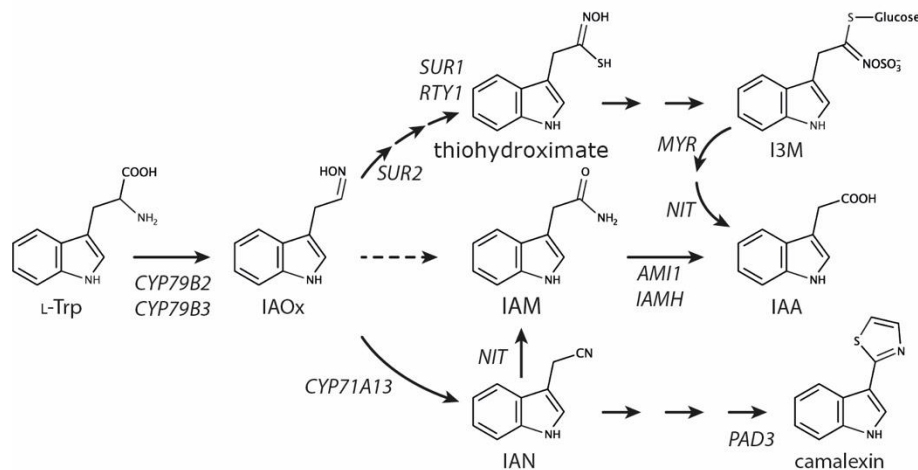

Figure 1. Metabolic pathways of the indole-3-acetaldoxime shunt in *Arabidopsis thaliana*. Schematic overview of the biosynthesis of L-Trp derived indole glucosinolate, camalexin, and indole-3-acetic acid. Dashed lines indicate reaction steps for which corresponding genes/enzymes have not yet been identified. *AMI1, AMIDASE1; CYP71A13, CYTOCHROME P450 MONOOXYGENASE 71A13, CYP79B2, CYTOCHROME P450 MONOOXYGENASE 79B2, CYP79B3, CYTOCHROME P450 MONOOXYGENASE 79B3,* I3M, glucobrassicin; IAA, indole-3-acetic acid; IAM, indole-3-acetamide; *IAMH, IAM HYDROLASE1-2,* IAN, indole-3-acetonitrile; IAOx, indole-3-acetaldoxime; L-Trp, L-tryptophan; *MYR, MYROSINASE; NIT, NITRILASE1-3; PAD3, PHYTOALEXIN DEFICIENT3 (CYP71B15); RTY, ROOTY; SUR1, SUPERROOT1; SUR2, SUPERROOT2 (CYP83B1).*

IAOx is considered to be an important metabolic branching point, involved in connecting primary and secondary metabolism [9-11]. Remarkably, IAOx serves as the common biochemical source for the formation of L-Trp derived glucosinolates [12], such as glucobrassicin, and camalexin [13], two important plant defense compounds in Arabidopsis. The formation of both metabolites is induced in response to biotic stresses and involves the transcription factors MYB34, MYB51, MYB122 and WRKY33 for the control of indole glucosinolate and camalexin biosynthesis, respectively [14,15]. The *cyp79b2/cyp79b3* double mutant, deficient in the formation of IAOx, shows a wild type-like phenotype and unaltered IAA levels under normal growth conditions [9,10,16], but demonstrates a significantly increased susceptibility towards pathogens [17], which underscores the importance of the IAOx pathway for biotic stress responses. Furthermore, *cyp79b2/cyp79b3* has been reported to contain drastically reduced indole-3-acetamide (IAM) contents, suggesting that a large proportion of IAM in Arabidopsis originates from IAOx [10]. IAM has, however, been found in several non-Brassica plant species and, therefore, do not possess the IAOx pathway [18]. Hence, it must be concluded that there is another biosynthetic route leading to IAM, possibly through yet unidentified tryptophan 2-monooxygenases in plants that share homology with known from enzymes from bacteria, such as iaaM or tms1 [19,20].

Indole glucosinolate biosynthesis mutants such as *sur1/rty* and *sur2* are, on the other hand, characterized by strongly increased auxin contents and high-auxin phenotypes [21-23]. Mass spectrometric analyses demonstrated a significant increase of IAOx, IAM, and IAA in *sur1-1*, while indole-3-acetonitrile (IAN) levels appeared unchanged [10], which is suggestive for a redirection of the metabolic flux into the IAM pathway.

Increased IAM level in *ami1* mutants have recently been shown to trigger abscisic acid (ABA) biosynthesis through the induction of *NCED3*, encoding for a key enzyme in the formation of ABA [24]. Along with the observation that IAM represses the expression of the K$^+$ transporters *HAK/KT12* and *KUP4* that are assumed to contribute to elongation growth [25], this led to the hypothesis that the conversion of IAM to IAA catalyzed by IAM hydrolases represents a molecular nexus involved in the crosstalk between auxin and ABA. Although the transcriptomics analysis provided conclusive evidence for an intimate connection of AMI1-mediated IAM conversion and abiotic stress responses, the molecular mechanism by which changes in IAM levels are perceived and integrated remain largely elusive.

Here, we characterize the impact of the simultaneous genetic blockade of the indole glucosinolate and IAM pathways in *A. thaliana*. By phenotypically and mass spectrometrically analyzing an *ami1/rty* double mutant, we demonstrate that accumulating IAM exerts a negative impact on embryo development. In addition, we report the comprehensive transcriptomics analysis of the mutant, which provided evidence for a number of physiological processes that are affected by the elevated IAM level in the mutant.

2. Results

2.1. The introgression of the ami1-2 mutation into rty1-1 is not sufficient to restore the wild type phenotype

Previous reports highlighted significant alterations in metabolite fluxes in indole glucosinolate biosynthesis mutants, including *sur1/rty* and *sur2*. The experiments suggested an accumulation of IAOx and its further channeling into IAA [22,23,26-28]. While the *cyp79b2/cyp79b3* double mutant that is practically devoid of IAOx shows wild type IAA levels, downstream mutations in *sur1* translate into significantly increased IAOx, IAM, and IAA contents, suggesting the channeling of IAOx into IAA to proceed via IAM (Figure 1) [10]. The significantly elevated IAA levels in those mutants provoke strong auxin overproduction-related phenotypes, including epinasty of cotyledons and true leaves, significant amplification of lateral root numbers, and an increased root hair number and density [21,23].

Picking up on these lines of evidence, which suggest a purely auxin-mediated phenotype, we reasoned that a genetic block of the IAM pathway (IAOx→IAM→IAA) in indole glucosinolate mutants may restore a wild type (wt) phenotype, due to the impaired conversion of IAM to IAA. To this end, we introgressed the *ami1-2* mutant allele into the *rty1-1/+* genetic background. After two rounds of selfing, we selected for plants homozygous for the *ami1-2* mutation using PCR genotyping. Subsequently, three lines homozygous for *ami1-2* were selected and subjected to cDNA sequencing of the *RTY* gene (At2g20610), in order to genotype the zygosity state of the *rty1-1* mutation in these lines. Since *rty1-1* originates from an ethylmethane sulfonate (EMS) mutagenesis approach, sequencing was necessary to genotype the state of the *rty1-1* mutation in the selected lines. As can be taken from Figure 2, two of the selected lines, line 5 and line 15, appeared to be homozygous *ami1/rty* double mutants. At the protein level (Figure 2b), the *RTY1-1* point mutation translates into a P213S amino acid exchange [29], which is likely to cause major structural changes in the RTY enzyme. Protein modelling of RTY and *RTY1-1* against the 1.7 Å crystal structure of a closely related prephenate aminotransferase from Arabidopsis [30] (PDB: 6F5V) and subsequent structure predictions suggested the loss of one α-helix motif in *RTY1-1* (13 α-helices) relative to the wild-type protein (14 α-helices) in the C-terminal part of the protein.
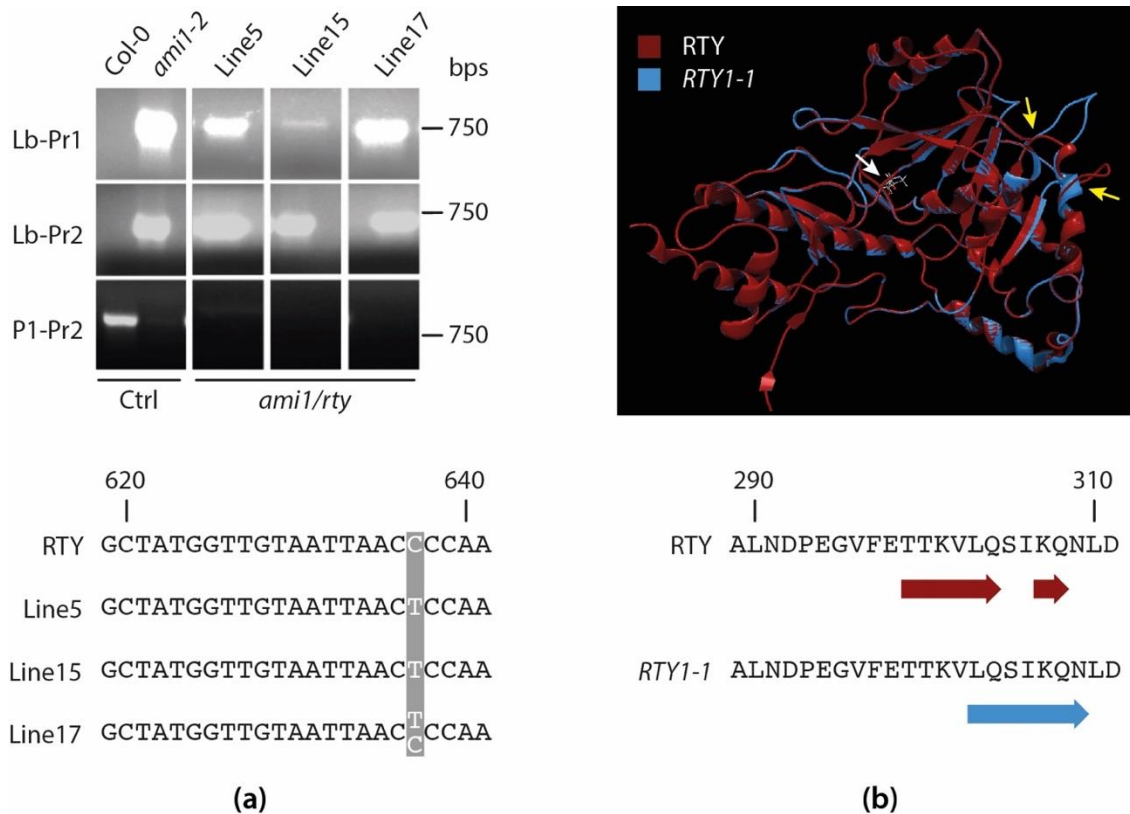
Figure 2. Genotyping of *ami1/rty* mutants. **(a)** PCR analysis comparing three selected double mutant lines with wt (Col-0) and *ami1-2* control (Ctrl) seedlings. The figure shows the results of three individual PCR reactions using either a T-DNA specific primer (Lb) and a 5' *AMI1*-specific primer (Pr1), a T-DNA specific primer (Lb) and a 3' *AMI1*-specific primer (Pr2) or the two *AMI1*-specific primers, Pr1 and Pr2 (upper panel). Section of the alignment of the annotated *RTY* cDNA with the sequences obtained from the sequencing of three selected mutants homozygous for the *ami1-2* mutation. The figure shows the point mutations at position 637 in lines 5 and 15 (grey box). The analysis of the trace files of line 17 revealed the heterozygosity of this line. Our results confirm the previously described point mutation for *rty1-1* (C→T)$_{637}$ [29]. Nucleic acid positions in the cDNA section are indicated (lower panel). **(b)** Overlay of the RTY (red) and *RTY1-1* (blue) 3D models (upper panel). The loop section comprising the P213S mutation (white arrow) and the altered α-helical structure (yellow arrows) are indicated. The lower panel additionally highlights the observed secondary structure changes.

Against our initial expectations, the *ami1/rty* double mutants still showed an auxin overproduction-related phenotype (Supplementary Figure S1), suggestive of a remaining conversion of IAM to IAA. This observation is in line with the recent identification of two additional acetamidase/formamidase family proteins described to act as IAM amidohydrolases in Arabidopsis [31]. Hence, it is plausible that the two IAM amidohydrolases, IAMH1 and IAMH2, are responsible for the remaining conversion of accumulating IAM to IAA. Interestingly, transcriptomics data from the presumably IAM accumulating *sur2* mutant and *iaaM* overexpressing tomato plants provide no indication for transcriptional alterations of the IAM amidohydrolase genes [32,33]. Along with the findings that IAM application triggers strong auxin-related root phenotypes in wild-type Arabidopsis and conditional *AMI1* overexpressor lines [24] and combined with the observation that Arabidopsis plants overexpressing the bacterial tryptophan 2-monooxygenase *iaaM* gene, producing IAM from L-Trp, also show considerable IAA and IAM overproduction [34,35], it must be concluded that Arabidopsis plants maintain a basal level of IAM amidohydrolases that readily convert accumulating IAM to IAA.

2.2. The ami1/rty double mutant is compromised in germiation

When further analyzing the offspring of the two identified *ami1/rty* double mutants, we found a severe impairment of the germination process for both lines. The obtained seeds did either not germinate at all or aborted germination after a very short period of time, ranging between 48 and 72 h, shortly after radicle protrusion through the seed coat (Figure 3a).
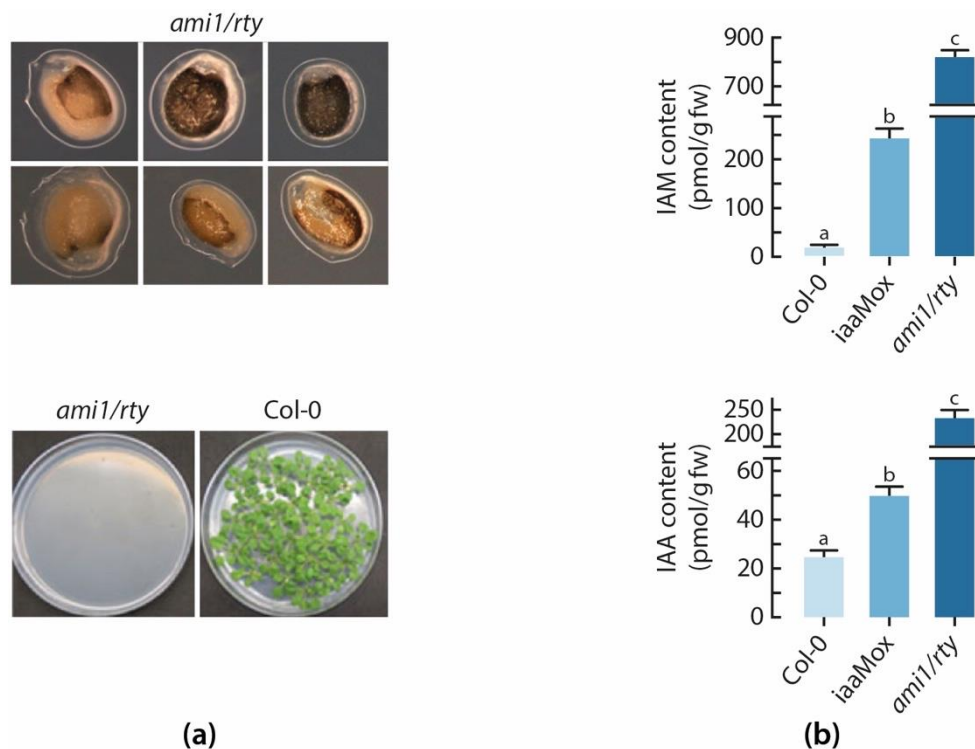

Figure 3. Seeds of *ami1/rty* mutants show a severe growth arrest and accumulation of IAM and IAA. **(a)** The photographs show close-ups of *ami1/rty* seeds grown on ½ MS plates (upper panel) and the comparison of wt (Col-0) and *ami1/rty* mutant seeds grown on ½ MS plates (lower panel). The *ami1/rty* seeds abort germination shortly after the radicle broke through the seed coat, while wt seeds (Col-0) were able to germinate. **(b)** Analysis of IAM and IAA levels in wild-type Arabidopsis, iaaMox, and *ami1/rty*. Imbibed seeds from wild-type Arabidopsis (Col-0), iaaMox, and the *ami1/rty* double mutant were analyzed for their endogenous IAM (upper panel) and IAA levels (lower panel). The plots show mean values with their corresponding standard errors (SE), n = 5. To assess significant differences between the endogenous levels of each compound an analysis of variance (ANOVA) of the scores followed by Tukey's *post-hoc* test was performed. The different letters indicate significant differences, $p \leq 0.001$.

The mass spectrometric analysis corroborated the high-auxin phenotype, providing evidence for a significant 10-fold increase of IAA levels in imbibed *ami1/rty* seeds compared to wt seeds. This underscores the notion that IAMH1 and IAMH2, respectively, contribute to the conversion of IAM to IAA in Arabidopsis. The iaaMox seeds, on the other hand, displayed an only 2-fold increase of endogenous IAA levels relative to wt. With respect to the IAM contents, it became evident that *ami1/rty* seeds accumulate over 45-times the amount of IAM of wt seeds. In agreement with previously published data of IAM contents in conditionally *iaaM* overexpressing seedlings [35], the iaaMox seeds showed a significant accumulation of IAM (14-times). With respect to the data published for *sur1-1* [10] that reported a 34- and 21-fold increase of endogenous IAM and IAA levels, respectively, the presented data underscore the role of AMI1 in the conversion of IAM to IAA in Arabidopsis. Apparently, the introgression of *ami1-2* into the *rty1* indole glucosinolate biosynthesis mutant background considerably altered the conversion of IAM into IAA and led to an enhanced accumulation of IAM.

Auxin has been described to control seed dormancy in Arabidopsis through the interaction with ABA signaling in an ABI3-dependent manner [36]. Elevated IAA contents were shown to increase the dormancy in transgenic iaaMox seeds. In order to exclude dormancy effects through the significantly increased IAA level in the double mutant, we tried different stratification periods, ranging between 2 to 6 days, but under none of the tested conditions, we were able to rescue *ami1/rty* mutant plants. However, given that most seeds were able to initiate germination, it must be concluded that seed dormancy is not the decisive factor responsible for the observed abortion of the germination process in the double mutants.

2.3. Alterations in cellular IAA and IAM contents impact embryo size in Arabidopsis

It is widely accepted that auxin synthesized by fertilized achenes drives fleshy fruit development and ripening, e.g. in strawberries [37-39], and that genetic boosting of auxin formation in ovules through the tissue-specific expression of the *iaaM* gene promotes parthenocarpy in tobacco, eggplant, and tomato [40-42]. The role of auxin in regulating seed development in dry dehiscent fruits, such as in the model plant Arabidopsis, is still less well understood, although great progress has been made over the past years [43-45]. In previous studies, we observed that the overproduction of IAA in Arabidopsis significantly increased seed size, while the accumulation of IAM was shown to reduce it [24,25]. Auxin has also been demonstrated to significantly impact seed size and starch accumulation in pea [46]. In Arabidopsis, the embryo takes up large part of the space in the seed and, thus, greatly determines seed size, as the endosperm is reduced to a single cell layer [47]. In order to quantify the effect of altered IAA and IAM contents on seed development, we compared the embryo sizes of a number of auxin biosynthesis-related mutants in comparison to wt embryos (Figure 4).
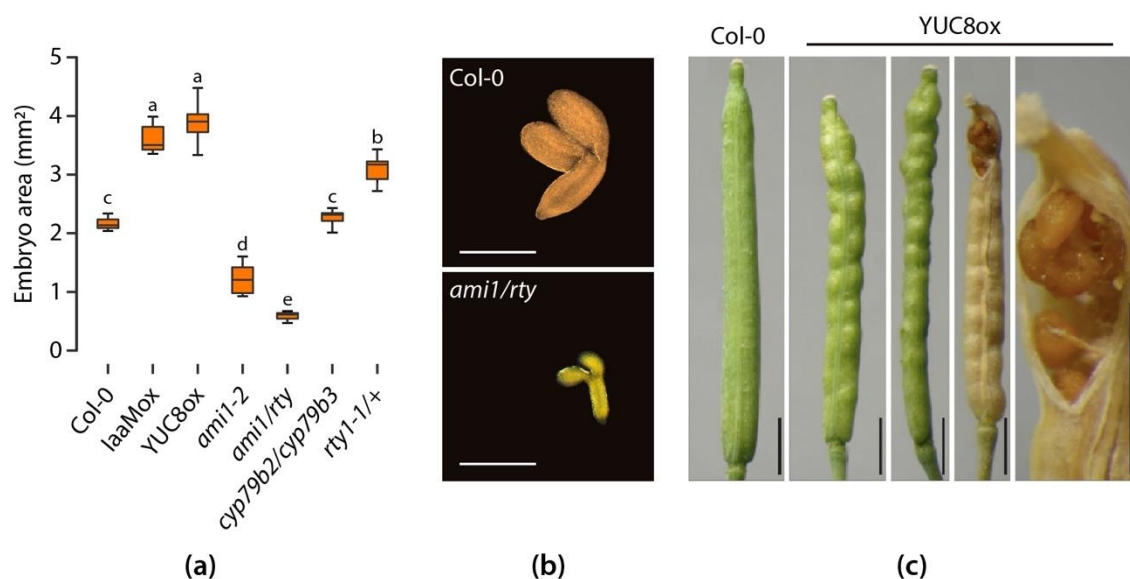

Figure 4. Effect of auxin on embryo and seed size in auxin mutants. (**a**) The box plots show the comparison of the embryo area of different auxin-related mutants. (**b**) Representative photographs of an *ami1/rty* embryo in comparison to wild type (Col-0). Both photographs have the same scale, scale bars = 1 mm. (**c**) Representative pictures of siliques from Col-0 and YUC8ox plants. Scale bars = 5 mm.

As displayed in Figure 4, embryos of auxin overproducing YUC8ox and iaaMox lines [34,48] were significantly bigger than wt embryos, whereas the IAM accumulating *ami1* embryos [24] appeared to be considerably smaller. This confirmed our previous findings and highlighted the already well-recognized growth promoting effect of auxin in fruit development. The effect on seed development in YUC8ox was so strong that the siliques were not able to follow the increased seed growth which, in consequence, resulted in the premature opening of the valves of non-dehiscent siliques along the replum (Figure 4c). At the same time, our results suggested that either the excessive accumulation of IAM or the partially blocked conversion of IAM to IAA in the *ami1* mutant have

growth inhibiting effects. Interestingly, the *rty* mutant [23,49], which is allelic to *superroot1* (*sur1*) [21], showed a slightly bigger embryo size than wild-type Arabidopsis. The *rty* seedlings are known to have elevated IAA contents [23], and can be expected to also have strongly elevated IAM levels, like *sur1* [10]. Taking the heterozygosity of the tested *rty1-1* seeds into account, the *rty1-1* embryos resemble those of iaaMox, that also contain elevated IAM and IAA level [19,34]. The largely IAM deficient *cyp79b2/cyp79b3* double mutant displayed no significant alteration of embryo size, which can likely be attributed to the wt IAA levels in this mutant [9,10,16]. Most remarkably, however, was the strong embryo phenotype of the *ami1/rty* double mutant. Potentiating the *ami1-2* embryo phenotype previously described [24], the *ami1/rty* double mutant embryos showed to be significantly smaller than wt and *ami1-2* embryos (Figure 4a,b).

2.4. The ami1/rty mutant shows major impairments in gene transcription and protein synthesis

Considering the drastic curtailing of embryo growth in the *ami1/rty* double mutant and the detected significant accumulation of IAM in the mutant seeds, we concluded that the canalization of IAM into IAA during seed filling must be an important factor for proper seed development. It seems as if the excessive accumulation of IAM triggers limited embryo development, while the observed growth arrest of the *ami1/rty* mutants during the germination process is possibly attributable to the limitation of storage compounds in the seed. To address the question what molecular processes are affected and responsible for the strong phenotype, we decided to take a comprehensive transcriptomics approach, comparing the transcriptional profile of *ami1/rty* mutant seeds with that of wt seeds by RNAseq. First, we analyzed the expression levels of 128 selected auxin metabolism-, signaling-, and transport-related genes in the *ami1/rty* mutant relative to wt (Table 1).

Table 1. Expression levels of selected auxin-related genes in the *ami1/rty* double mutant versus wt.

Gene	*log2FC*	FDR	Gene	*log2FC*	FDR
Auxin biosynthesis			**Auxin transport**		
At4g24670 (*TAR2*)	-0.28	0.84	At2g38120 (*AUX1*)	-0.66	0.83
At4g13260 (*YUC2*)	4.70	0.58	At5g01240 (*LAX1*)	3.81	0.81
At1g04610 (*YUC3*)	0.52	0.79	At2g21050 (*LAX2*)	-0.82	0.87
At5g11320 (*YUC4*)	4.39	0.84	At2g36910 (*PGP1*)	-0.15	0.80
At5g25620 (*YUC6*)	-0.56	0.82	At3g28860 (*PGP19*)	0.57	0.75
At4g28720 (*YUC8*)	-0.63	0.81	At1g73590 (*PIN1*)	-0.83	0.70
At1g48910 (*YUC10*)	0.14	0.96	At5g57090 (*PIN2*)	0.91	0.59
At1g08980 (*AMI1*)	**-1.15**	**0.05**	At1g70940 (*PIN3*)	-0.98	0.67
At4g37550 (*IAMH1*)	-0.88	0.77	At2g01420 (*PIN4*)	0.21	0.95
At4g37560 (*IAMH2*)	-0.01	0.99			
At4g39950 (*CYP79B2*)	4.59	0.58	**Auxin signaling**		
At2g22330 (*CYP79B3*)	-3.46	0.81	At3g62980 (*TIR1*)	0.20	0.61
At2g44310 (*NIT1*)	-0.16	0.56	At3g26810 (*AFB2*)	-0.49	0.61
At3g44300 (*NIT2*)	0.17	0.63	At1g12820 (*AFB3*)	-0.70	0.34
At3g44320 (*NIT3*)	-0.13	0.75	At4g02980 (*ABP1*)	-0.75	0.10
			At3g23030 (*IAA2*)	0.49	0.17
Auxin conjugation/degradation			At1g04240 (*IAA3*)	0.22	0.96
At1g24180 (*IAR4*)	-0.08	0.81	At5g43700 (*IAA4*)	-4.25	0.79
At5g56650 (*ILL1*)	-1.16	0.77	At1g15580 (*IAA5*)	-5.13	0.77
At5g54140 (*ILL3*)	-1.43	0.75	**At5g65670 (*IAA9*)**	**-0.39**	**0.03**
At1g51780 (*ILL5*)	-3.81	0.83	**At1g04550 (*IAA12*)**	**-2.02**	**0.02**

Gene	*log2FC*	FDR	Gene	*log2FC*	FDR
At3g02875 (*ILR1*)	0.07	0.86	At4g14550 (*IAA14*)	1.24	0.82
At4g15550 (*IAGLU*)	**-1.25**	**>0.01**	At3g04730 (*IAA16*)	4.25	0.75
At2g14960 (*GH3.1*)	0.11	0.93	At2g46990 (*IAA20*)	-0.84	0.87
At4g27260 (*GH3.5*)	**1.63**	**0.05**	At5g25890 (*IAA28*)	-1.84	0.69
At5g54510 (*GH3.6*)	1.72	0.68	At2g33860 (*ARF3*)	-0.98	0.67
At1g14130 (*DAO1*)	-0.31	0.76	At1g19850 (ARF5)	-2.59	0.82
At1g14120 (*DAO2*)	0.22	0.97	At5g20730 (ARF7)	0.06	0.88
			At5g37020 (ARF8)	0.18	0.95
Glucosinolate and camalexin biosynthesis			At4g23980 (ARF9)	0.02	0.92
At2g30770 (*CYP71A13*)	3.91	0.78	At2g46530 (ARF11)	0.74	0.49
At2g20610 (*RTY*)	**-0.45**	**0.05**	At1g34310 (ARF12)	3.81	0.83
At4g31500 (*SUR2*)	-0.97	0.61	At4g30080 (ARF16)	0.23	0.68
At1g24100 (*UGT74B1*)	**1.08**	**0.01**	At1g19220 (ARF19)	0.66	0.32
At1g59870 (*PEN3*)	0.34	0.52	At1g43950 (ARF23)	5.25	0.81
At5g60890 (*MYB34*)	5.12	0.58	At5g17430 (*PLT4*)	0.65	0.73
At1g18570 (*MYB51*)	4.86	0.58	**At5g57390 (*PLT5*)**	**-0.51**	**>0.01**
At2g38470 (*WRKY33*)	**0.98**	**>0.01**	At4g37650 (*SHR*)	6.19	0.14

Genes that exhibit a significant difference in their expression are marked in bold letters.

The directed assessment of target gene expression levels revealed that genes associated with auxin *de novo*-biosynthesis were not significantly altered in their transcription. This underpins that the high auxin contents in the mutant must derive from the genetic block of indole glucosinolate biosynthesis and the remaining flux of IAM to IAA, and that alteration of *de novo* auxin biosynthesis is not involved. At the same time, we found a significant induction of the Gretchen Hagen gene *GH3.5*. *GH3.5* encodes an acyl amino synthetase that preferentially conjugates IAA to aspartate if IAA and Asp contents are high [50]. This may be interpreted as a response to counteract the high IAA contents in the mutant. Inconsistent with this notion of buffering high IAA contents through conjugation, we determined the significant repression of an UDP-glucose:indole-3-acetate ß-D-glucosyltransferase (*IAGLU*). IAGLU is assumed to be capable of glycosylating IAA [51], as it shares homology with known IAGLUs from maize [52]. However, the *in vivo*-function of IAGLU from Arabidopsis is yet to be elucidated, particularly because another publication described an enzymatic activity of IAGLU towards kaempferol [53]. Thus, IAA may not be the endogenous substrate for IAGLU *in vivo*. With respect to the biosynthesis of L-Trp derived defense compounds, i.e. camalexin and indole glucosinolate, we were not able to find conclusive evidence for the redirection of the metabolic flux into the biosynthesis of camalexin. Consistent with the role of the significantly induced transcription factor *WRKY33* as negative regulator of camalexin biosynthesis [15], we registered no induction of camalexin biosynthesis-related genes, such as *CYP71A13* and *PAD3*. Hence, it must be concluded that there is no alternative metabolic bypass and the entire metabolic flux normally directed into indole glucosinolate biosynthesis now passes through the IAM shunt. Additionally, we detected no significant changes in the expression of auxin transport-related genes, and only the *IAA9*, *IAA12/BODENLOS (BDL)*, and *PLETHORA5 (PLT5)* transcriptional regulators appeared to be differentially expressed in the mutant. While the reduced expression of *IAA9* and *PLT5* may be neglected because of their only minor differential expression, the repression of *IAA12/BDL* was far more pronounced. IAA12/BDL is known to affect primary root formation and apical-basal patterning in embryos [54]. Aux/IAA auxin signaling repressor proteins act in response pairs with their particular auxin response factor (ARF) transcription factors. IAA12/BDL is described to closely interact with MONOPTEROS (ARF5) [55,56]. Hence, the transcriptional repression of *IAA12/BDL*

may result in an increased amount of free ARF5, because of a reduced recruitment of the transcription factor by its transcriptional repressor into inactive heterocomplexes. However, apical-basal pattern formation is apparently no issue in *ami1/rty*, as the embryos showed a clear polar organization (Figure 4b).

Since our targeted approach did not disclose auxin related processes that could explain the embryo and germination phenotype of *ami1/rty*, we next undertook an in-depth transcript profiling approach to obtain a broader picture of differentially expressed genes (DEGs) and their functional relationships. Employing an adjusted *p*-value (FDR) of < 0.05 and an arbitrarily chosen differential expression value of *log2FC* ≥ +1 for induced genes and *log2FC* ≤ -1 for repressed genes, respectively, 101 induced and 564 repressed DEGs were identified (see Supplementary table S1). To functionally score the DEGs, we used the MapMan software. The application returned a small number of key processes that are affected in the double mutant. These processes include RNA processing, ribosome assembly, nucleotide metabolism, translation, as well as protein modification and degradation. In addition, the results pointed towards the transcriptional alteration of stress response-, signaling-, and transport-related genes (see Supplementary table S1).

With the aim to gain more detailed insight into the relationships of the selected DEGs, we performed a functional association network analysis. For the induced DEGs, we obtained a network with 94 nodes and 62 edges. Further analysis of the network, focusing on the node with the highest degree of connectivity, *WRKY40*, provided a subnet with 8 nodes and 15 edges. Along with the genes *ZAT7*, *CML37*, *AOX1A*, and *ACS6*, the central *WRKY40* hub could be associated with oxidative stress responses, while its association with *SYP121* and the glycolipid transfer protein gene *At4g39670* pointed towards an additional role in cell membrane organization. When searching for the nodes with the highest betweenness centrality, we identified the transcription factor *FUS3*, which appeared to be connected in a small sub-network with the seed storage albumin genes *SESA2* and *SESA4*, as well as with the fatty acid desaturase *FAD2*. From this it may be concluded that seed storage protein biosynthesis is sought to be induced in the double mutant, but the comprised translational machinery in this mutant inhibits the process. For the downregulated DEGs, we inferred a network with 554 nodes and 7128 edges. The gene with the highest degree of connectivity was the ribosomal protein gene *REDUCED POLLEN NUMBER 1 (RDP1)* [57] with 140 connections, followed by the ribosome biogenesis related *FIBRILLARIN 2* (*FIB2*) gene [58] and the *RIBOSOMAL LARGE SUBUNIT 4* (*RPL4*) gene with 138 and 133 connections, respectively. RPL4 is a particularly interesting candidate, because it has been associated with auxin-regulated developmental processes, endomembrane trafficking, and lipid metabolism [59]. However, from a more general perspective, the network analysis referred to an impairment of ribosome-dependent processes, which confirms the previously discussed classification of the DEGs. The Kyoto Encyclopedia of Genes and Genomes (KEGG) [60] pathway enrichment analysis of the three mentioned sub-networks also highlighted ribosome- and ribosome biogenesis-related processes to be underrepresented in the *ami1/rty* mutant (Supplementary Figure S2). Among the downregulated DEGs, the genes *NITRATE REDUCTASE 1* (*NIA1*), *PHOSPHOGLUCOSE ISOMERASE 1* (*PGI1*), and the uridine 5'-monophosphate synthase gene *At3g54470* showed the highest betweenness centrality. On the basis of the topology of the extracted network for the three central hubs, we performed a KEGG pathway enrichment analysis. As can be taken from Figure 5, the network inferred from the betweenness centrality in combination with a projection onto the KEGG pathway maps identified a series of metabolic routes, including amino acid and carbon metabolism pathways, that are seemingly affected in the *ami1/rty* double mutant.
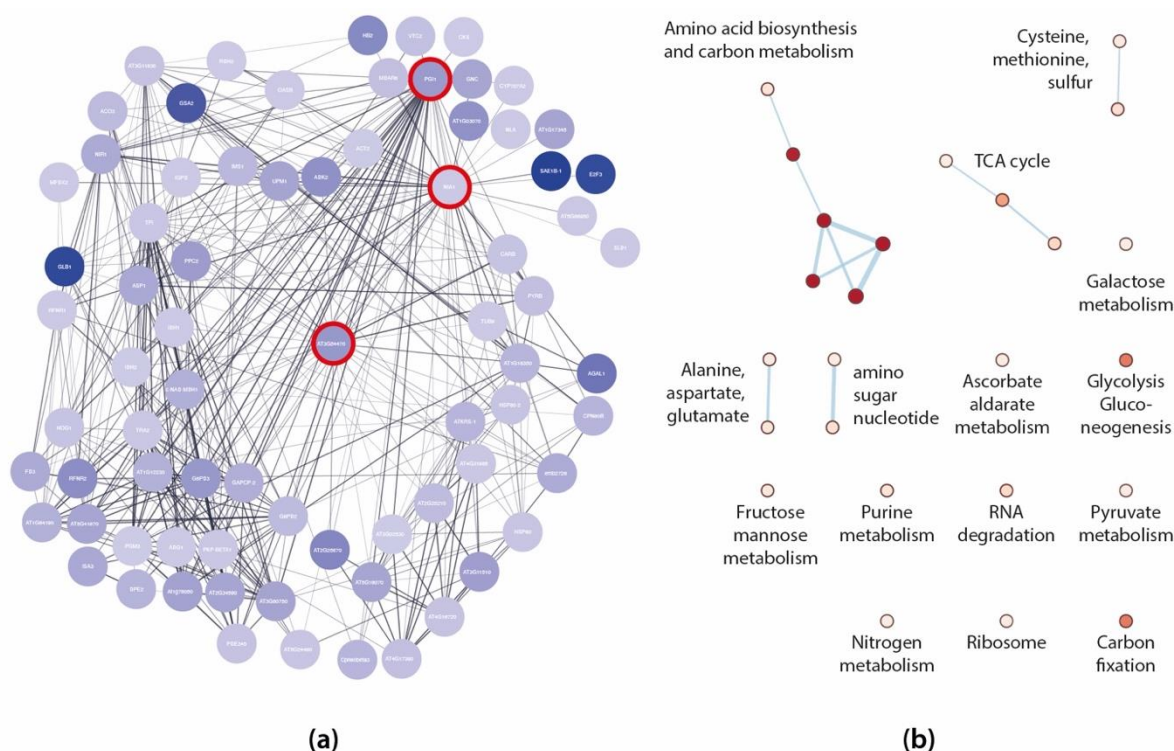
Figure 5. Network analysis of downregulated DEGs in *ami1/rty*. (**a**) Extracted network for the three DEGs with the highest betweenness centrality. The central hubs *NIA1*, *PGI1*, and *At3g54470* are highlighted by red circles. The nodes are color coded according to the *log2FC* expression levels of the DEGs (white to blue), with dark blue marking the most repressed DEGs. Edge thickness reflects the betweenness score between the nodes. (**b**) KEGG pathway enrichment analysis of the sub-network extracted for *NIA1*, *PGI1*, and *At3g54470*. The color (white to red) gives account on the normalized enrichment score of the corresponding KEGG pathways.

Most remarkable, however was the high betweenness centrality of *NIA1. NIA1* encodes the cytosolic minor isoform of nitrate reductase *NIA2* and accounts for about 15% of the nitrate reductase activity in plants [61]. Nitrate reductases and nitrite reductases catalyze the first two consecutive steps of nitrate assimilation in plants, a process that is closely related with the biosynthesis of amino acids.

Gene Ontology (GO) biological process terms represent a rich resource for the functional characterization of large 'omics' data sets. GO annotations include a mix of manually curated and electronically inferred sources [62]. Taking advantage of this resource, we next subjected the previously derived functional association networks for both up- and downregulated DEGs to a GO enrichment analysis. As demonstrated in Figure 6, the inferred GO enrichment map largely confirmed the previously obtained results, highlighting a significant underrepresentation of biological processes related with translation, including ribosome biogenesis and assembly, rRNA processing, and ribonucleotide biosynthesis. However, in addition to these already discussed processes, the GO enrichment analysis provided additional evidence for the underrepresentation of some interconnected seed development- and germination-related terms, while a small number of GO terms associated with seed maturation appeared to be overrepresented. Most notably, the study brought additional insight into the enrichment of GO classifications associated with drought and osmotic stress responses to light. Moreover, it highlighted the impairment of the temperature stress response in *ami1/rty*.
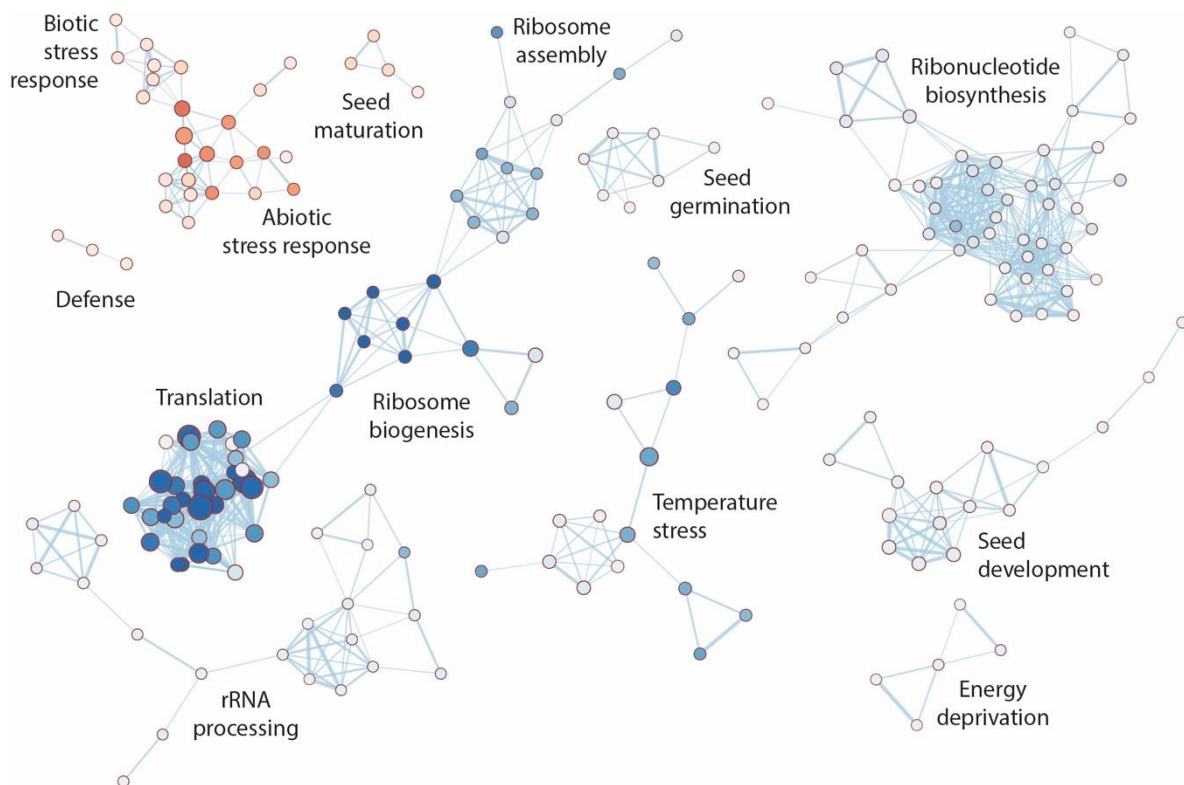
Figure 6. GO term enrichment map for up- and downregulated DEGs. GO terms that share members are shown in connected clusters. Cluster labels were retrieved using the AutoAnnotate v1.3.3 application in Cytoscape. The node color reflects the normalized enrichment score with underrepresented terms represented in blue and overrepresented terms given in red. The node size gives account on the number of members in the particular GO term.

Among the overrepresented abiotic stress related genes, the cell wall remodeling associated *EARLY RESPONSE TO DEHYDRATION (ERD7)* [63,64] gene, the transcription factor *ZAT10 [65]*, and the galactinol synthase gene *GOLS2* [66] are noteworthy. All three genes have been demonstrated to play central roles in responses to drought and salt stress in Arabidopsis. Their induction may suggest that the mutant plant is prone to drought stress, as it is possibly not able to efficiently control its water balance over the course of seed development. This argument is further strengthened by the observed induction of *FUSCA 3* (*FUS3*) in the mutant. FUS3 is an ABA-responsive master regulator of seed development and essential for the establishment of desiccation tolerance in seeds [67], including the substantial induction of *LATE EMBRYOGENESIS ABUNDANT PROTEIN* (*LEA*) genes [68]. Intriguingly, an intimate relationship between IAM accumulation in the *ami1* mutants and the induction of ABA biosynthesis and downstream regulatory processes has just recently been reported [24].

With respect to the repressed genes falling into the seed development and germination clusters, the ABC transporter gene *ABCG11*, which contributes to cutin and suberin metabolism as well as to reproductive organ development [69], and the WDxR motif–containing protein gene *WDR55* that is involved in the control of seed development [70] have to be mentioned. In addition, we registered the significant downregulation of the *S*-adenosyl-L-homocysteine hydrolase *HOG1*. HOG1 is known to interact with the likewise repressed *RECEPTOR FOR ACTIVATED C KINASE 1A* product RACK1 [71], and *hog1* knockout mutants are described to have an embryo growth arrest at the globular stage [72]. The downregulation of the HOG1 hub may contribute to the curtailed embryo development of the *ami1/rty* mutant. Moreover, we identified *SLEEPY1* (*SLY1*) as a potentially interesting candidate. *SLY1* encodes a F-box protein that targets gibberellin signaling repressors and, thus, interferes with the gibberellin response [73]. Intriguingly, *sly1-10* mutants exhibit a dwarfish phenotype, and many *sly1-10* plants were infertile, which leaves room for the speculation of the contribution of *SLY1* and downstream alterations in the crosstalk with gibberellins to the *ami1/rty* phenotype.

2.5. Hyperaccumulation of IAM provokes repression of cell proliferation and elongation growth regulatory pathways

In order to explore gene regulatory networks that are possibly involved in causing the *ami1/rty* embryo phenotype and to experimentally validate the conclusions drawn from the RNAseq experiment, we centered our interest on transcription factors with significantly altered expression levels. A compilation of these factors can be found in Supplementary Table S1. Overall, 34 transcription factors were identified, from which eight were significantly induced, while 26 appeared to be significantly repressed. As presented in Figure 7, ten of these genes were selected and their transcriptional response towards a short-term treatment with IAM was tested by qRT-PCR.
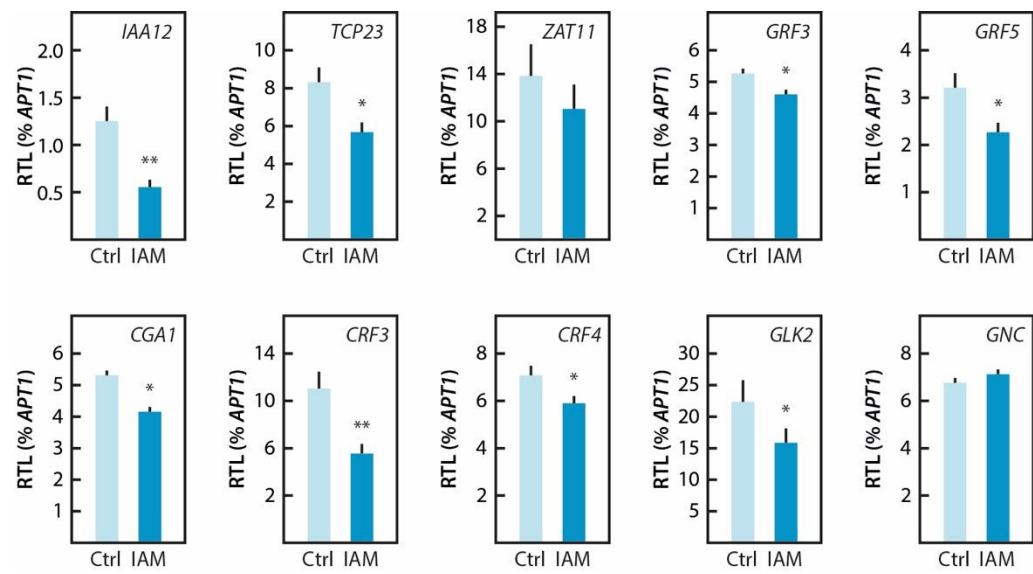

Figure 7. Validation of RNAseq data by qRT-PCR. The figure shows the relative transcript levels (RTL) of selected target genes (arithmetic mean ± SE, n = 9) normalized to *APT1* as a constitutively expressed control gene in 7-day-old wt (Col-0) seedlings. Before RNA extraction, the seedlings have either been treated for 2 h with 20 µM IAM (IAM) or with a control solution (Ctrl) free of IAM. The selected target genes were: *IAA12/BDL*, *Aux/IAA protein 12* (At1g04550); *TCP23*, *TEOSINTE BRANCHED 1/CYCLOIDEA/PROLIFERATING CELL FACTOR 23* (At1g35560); *ZAT11*, *ZINC FINGER TRANSCRIPTION FACTOR 11* (At2g37430); *GRF3*, *GROWTH REGULATING FACTOR 3* (At2g36400); *GRF5*, *GROWTH REGULATING FACTOR 5* (At3g13960); *CGA1*, *CYTOKININ-RESPONSIVE GATA FACTOR 1* (At4g26150); CRF3, *CYTOKININ RESPONSE FACTOR 3* (At5g53290); *CRF4*, *CYTOKININ RESPONSE FACTOR 4* (At4g27950); *GLK2*, *GOLDEN-LIKE 2* (At5g44190), and *GNC*, *GATA, NITRATE-INDUCIBLE, CARBON-METABOLISM INVOLVED* (At5g56860), in order of appearance. Asterisks indicate significant differences between the corresponding control sample and the IAM treated sample. (Student's *t*-test; *$p \leq 0.05$, **$p \leq 0.01$).

The most pronounced induction was registered for the *MYB4* gene, followed by *ZAT11*. MYB4 is a R2R3-subfamily MYB domain protein associated with radiation and thermal stress responses in Arabidopsis [74,75]. The induced Cis_2/His_2-type zinc finger proteins ZAT7 and ZAT11 are also associated with abiotic stress, particularly with responses to salinity stress and nickel tolerance, respectively [76,77]. Along with these genes we found a pronounced induction of the WRKY-domain protein gene *WRKY40*, which is reported to be involved in biotic stress responses and the control of indole glucosinolate biosynthesis [78,79]. Most interesting, however, is the link of *WRKY40* expression with ABA signaling in Arabidopsis and its control by the transcriptional regulators GOLDEN2-LIKE 1 and -2 (GLK1/2) [80], because increased IAM contents are known to trigger ABA biosynthesis [24] and *GLK2* was registered among the repressed factors.

Among the repressed factors, we also found several stress related target genes, such as the heat shock factors *HSFA2* and *-3*, implicated in thermotolerance and osmotic stress tolerance [81,82], as well as the cytokinin response factors *CRF3*, *CRF4*, involved in cold stress responses and freezing

tolerance in plants [83,84]. This further substantiates the tight connection between IAM accumulation and plant stress responses. In addition, we identified the significantly repressed *TEOSINTE BRANCHED 1/CYCLOIDEA/PROLIFERATING CELL FACTOR* genes *TCP4*, *TCP10*, and *TCP23* as potential targets. TCPs are reported to play pivotal roles in the control of morphogenesis of shoot organs and developmental processes, such as flowering [85,86]. Remarkably, however, is the direct connection of TCP4 and TCP10 with auxin homeostasis related processes, especially the induction of *YUC5* by TCP4 [87] and the downregulation of TCP4 and TCP10 in the *iamt1-D* gain-of-function mutant [88], which implies the existence of regulatory loops that connect developmental processes with endogenous auxin levels that possibly also involve the HD-ZIP protein HAT5.

However, two other groups of transcription factors, including the gibberellin signaling repressors *GNC*, *GNL/CGA1* [89], and the growth-regulating factors *GRF3* and *GRF5* that are recognized as mediators of organ size establishment and cell proliferation [90,91], attracted our interest, as they promised mechanistic insight into the crosstalk between IAM and gibberellin, as well as with general growth control.

In order to investigate as to whether IAM can trigger similar responses in wild-type Arabidopsis, we tested the gene regulatory effect of exogenously applied IAM in wild-type seedlings. Apart from the induced *ZAT11*, for which the induction could not be confirmed, we studied nine further genes repressed in *ami1/rty*. Except for *GNC*, the repression of all other selected genes by IAM could be confirmed by qRT-PCR analysis. However, it has to be remarked that the impact of the short-term IAM treatment was generally less pronounced than the effect observed in the RNAseq analysis of the *ami1/rty* double mutant.

3. Discussion

Auxins are well-characterized phytohormones that control a huge variety of different growth- and development-related processes. The role of auxin in pattern formation and embryogenesis has been studied in great detail [92,93]. Several recent publications ascribe auxin also an important role in later stages of seed development, including seed filling, dormancy control, and germination. An example is the pivotal role of local auxin biosynthesis in the endosperm for proper seed coat formation [94], the increased dormancy of IAA overproducing mutant plants [36], or the observed impact of reduced auxin formation on seed size growth and starch formation in legumes [46]. A similar positive regulatory relationship of auxin formation and starch production in rice has also been suggested [95]. On the other hand, nutrient allocation and plant hormone crosstalk are assumed to play essential roles in seed development as well. A number of K^+ channels and transporters are downstream targets of auxin [25], and auxin biosynthesis is reported to be controlled by sugars [96,97]. Most recent results give reason to speculate on an involvement of auxin-ABA crosstalk in this process [98,99]. However, overall, the role of auxin in orchestrating seed development has received only little attention, despite is undeniable role as key regulator of plant development. A more detailed analysis may entail biotechnological advances that could be harnessed to improve agricultural productivity in an environmentally friendly manner.

Our previous work shed some light on the role of IAA and its direct precursor, IAM, in seed development and a connection with phytohormone crosstalk [24,25,48,100]. Our findings led to the hypothesis that IAM is a negative plant growth regulator and that the enzymatic conversion of IAM to IAA by AMI1 terminates its growth inhibitory action. A similar function of another amidase signature family member, FAAH (FATTY ACID AMIDE HYDROLASE), has already been demonstrated. FAAH catalyzes the hydrolysis of *N*-acylethanolamines, which represent lipid signaling molecules, thereby controlling their action [101,102]. In this study, we aimed at addressing the question on the molecular and physiological consequences of endogenously accumulating IAM contents in Arabidopsis. For this reason, we decided to cross the indole glucosinolate biosynthesis mutant *rty1-1*, which has significantly elevated IAM and IAA levels, with the *ami1-2* mutant, to block the enzymatic conversion of IAM to IAA. Against our initial expectation, homozygous double mutants showed no wild-type phenotype and IAA levels, but resembled a mild *rooty* phenotype (Supplementary Figure S1) and were characterized by elevated IAA contents (Figure 3). However,

the observed remaining IAM hydrolase activity confirmed our previous observation of a remaining amidase activity in *ami1* mutants [24]. Moreover, it is in line with the recent identification of two additional enzymes, IAMH1 and IAMH2, that also contribute to the conversion of IAM to IAA in Arabidopsis [31]. Taking the reported remaining 40 to 45% IAM hydrolase activity of *ami1* mutants into account, the obtained data neatly reflect the loss of AMI1 activity in the mutant, particularly because only one of the two other amidases, *IAMH1*, shows expression during seed development [103].

To our surprise, seeds from the offspring of homozygous *ami1/rty* mutant plants showed to be nonviable, aborting germination shortly after the radicle broke through the seed coat. Given that the homozygous parent plants germinated normally and set a small number of siliques, it may be concluded that they derived from ancestors heterozygous for *rty*, and that, e.g., the nutrient acquisition during seed filling is compromised in the homozygous parents, which may explain the impairment of germination in the offspring. To gain closer insight into the embryo phenotype, we inspected the *ami1/rty* embryos and compared them to a series of other auxin biosynthesis-related mutant embryos. The quantitative assessment of the embryos disclosed a striking reduction of the size of *ami1/rty* mutant embryos. The phenotypic inspection was accompanied by the mass spectrometric analysis of IAM and IAA contents in the seeds. In comparison to the reported 34- and 21-fold increase of endogenous IAM and IAA levels in *sur1-1* mutant [10] that is allelic to *rty*, we found a 45- and 10-fold increase of endogenous IAM and IAA levels in double mutant seeds. From this, we conclude that the embryo phenotype of *ami1/rty* is likely attributable to the further elevated IAM contents. To obtain further insight into the role of IAM catabolism on seed development, it will be highly interesting to generate an *ami1/iamh1/iamh2* triple mutant in the future, although such mutants might be prone to nonviability.

With the objective to further our understanding about the molecular consequences of the observed IAM accumulation in the dwarfish *ami1/rty* mutant embryos, we subjected double mutant seeds to whole-genome transcript sequencing (RNAseq) and compared the obtained transcriptional profile with that of wild-type seeds. First, we checked the expression of a subgroup of 128 auxin-related genes. The targeted analysis provided no evidence for the misregulation of auxin metabolism-, transport-, or signaling-related genes. In particular, the missing activation of genes of the camalexin biosynthesis pathway is noteworthy, because we initially speculated that accumulation of IAOx or IAM may trigger a metabolic redirection into the camalexin pathway. On the contrary, we found the induction of *WRKY33*, a transcriptional repressor of camalexin biosynthesis (Table 1). The mRNA sequencing revealed, however, a significant downregulation of RNA processing- and translation-related genes. The mainly affected processes included ribosome biogenesis and assembly, as well as rRNA processing (Figure 6, Supplementary Table S1). A directed search for the differential expression of master regulators of ribosome biogenesis, such as *SMO4* (*SMALL ORGAN 4*) or *MAS2* (*MORPHOLOGY OF ARGONAUTE 1-52 SUPPRESSED 2*) [104,105], was however not successful. In addition, our network analysis of the expression data revealed that the *ami1/rty* mutant seeds fall significantly short in the expression of sugar and amino acid metabolism-associated transcripts. Considering the dwarfish embryo phenotype and impaired germination, we conclude that *ami1/rty* mutants are most likely compromised in seed filling. The major storage organ in Arabidopsis seeds are the cotyledons. The substantially reduced cotyledon size in the double mutant is suggested to prevent the deposition of adequate storage reserves (oil, protein, starch) in the seed, which ultimately leaves the germinating seedlings with insufficient energy resources to cover the initial growth phase until the seedlings establish an autotroph lifestyle.

The transcriptomics analysis provided additional evidence for the differential regulation of thermal, drought, and osmotic stress related genes. This observation matches well with our previous finding of an intimate connection between abiotic stress responses and increased IAM contents [24]. The misregulation of a substantial number of LEA protein genes and the involvement of drought stress related processes additionally point towards an important misregulation of the establishment of desiccation tolerance related processes. Of particular interest for our future work was, however, the identification of a number of plant growth regulating processes that were significantly repressed

in the *ami1/rty* double mutant. The repression of the growth-regulating factors *GRF3* and *GRF5* in IAM treated wild-type Arabidopsis seedlings confirmed a direct connection between IAM and the regulation of plant growth. In addition, our bioinformatics analyses brought a small number of plant hormone-regulatory circuits to light, which suggest an even more important role of IAM in plant hormone crosstalk, connecting with gibberellin signaling through the repression of *SLY1*, a F-box protein that targets gibberellin signaling repressors (DELLA proteins) [73], as well as *GNC* and *CGA1*, two transcription factors that act downstream of the DELLAs on gibberellin signaling [89], although the transcriptional repression by IAM was only confirmed for *CGA1*. Interesting was also the identification of the repression of the three TCP family members *TCP4*, *TCP10*, and *TCP23* that are assumed to play pivotal roles in the control of shoot morphogenesis and developmental transitions, such as flowering [85,86]. A significant repression of *TCP23* in wild type seedlings by IAM could be confirmed by transcript quantification. Particularly, the further investigation and elucidation of IAM perception and signaling will be a thrilling task for our future work.

4. Materials and Methods

4.1. Plant material and growth conditions

The presented experiments used the *Arabidopsis thaliana* Col-0 background (N1092) as reference. The *rooty* mutant (*rty1-1/+*, stock N8156) was obtained from the Nottingham Arabidopsis Stock Center (NASC). The mutants iaaMox [19,106], YUC8ox [48], *ami1-2* [24], and *cyp79b2/cyp79b3* [16] have previously been described in close detail. The *iaaMox* mutant [106] has been kindly provided by Dr. Yunde Zhao. The *ami1/rty* double mutant was generated by crossing the *ami1-2* mutant with *rty1-1/+* plants, followed by geno- and phenotyping of the offspring in the F2 and F3 generation, respectively.

Seedlings were grown under sterile conditions on solidified ½ MS-medium containing 1 % (w/v) sucrose in Petri dishes [107]; plantlets were kept under constant environmental short day conditions (8 h light at 24 °C, 16 h darkness at 20 °C, photosynthetically active radiation 105 μmol photons m^{-2} s^{-1} from standard white fluorescent tubes) for two to three weeks. Thereafter, plants were transferred to a mixture of soil and sand (2:1) and kept under long day conditions (16 h photoperiod) in a greenhouse, which was maintained under constant climatic conditions, 22 to 24 °C during daytime and 18 to 20 °C overnight. The photosynthetically active radiation was no less than 150 μmol photons m^{-2} s^{-1} (supplementary light, if required, from sodium-vapor lamps).

4.2. Genotyping of the ami1/rty *double mutant*

To genotype *ami1/rty* mutants, a two-step approach has been taken. First, the zygosity state of the *ami1-2* T-DNA integration was analyzed by PCR [108]. Instead of running a multiplex PCR with the two *AMI1*-specific primers Pr1/Pr2 and the T-DNA-specific primer Lb, we performed three independent reactions (Pr1/Pr2, Pr1/Lb, Pr2/Lb) for each selected line. After identifying lines homozygous for the *ami1-2* mutation, we extracted total RNA [109] and prepared cDNA libraries from those lines using M-MLV reverse transcriptase and oligo(dT)$_{15}$ primer according to the manufacturer's instructions. Next, we amplified the *RTY* gene using the primers RTY-fwd and RTY-rev by PCR. See Supplementary Table S2 for primer sequences. The obtained *RTY* PCR fragments of the three lines have then been sequenced on ABI 3730 xl sequencer by the company Stabvida. Sequence and trace file analysis have been carried out using the CLC Main Workbench 7.

4.3. Modelling of the RTY and RTY1-1 *protein structure*

The three-dimensional structures of RTY and *RTY1-1* were modeled by using the SWISS-MODEL interface (http://swissmodel.expasy.org) [110], utilizing the 1.7 Å crystal structure of a bifunctional aspartate aminotransferase and glutamate/aspartate-prephenate aminotransferase (PAT, At2g22250) deposited in the RCSB Protein Data Base (PDB: 6F5V) [30]. In accordance with [29], we used the PAT structure as template, although RTY is structurally closely related with alanine aminotransferases, e.g. from *Hordeum vulgare* (PDB: 3TCM), because this crystal structure originates

from the same species. Structural examination was performed using either PyMOL v1.47 or CLC Main Workbench 7.

4.4. Quantitative comparison of embryo sizes

Dry seeds from wild-type Arabidopsis and the different auxin mutant lines were surface sterilized using successive treatments with 70% ethanol (v/v, 5 min) and a 5-7% sodium hypochlorite solution (v/v, 5 min), before being rinsed three times with water. Afterwards, the seeds were left overnight at 4 ºC in DEPC water. Under a binocular (Leica MZ10 F), seeds were then transferred onto an object slide and mixed with glycerol. After removing the seed coat from the embryo, pictures were taken with 25-fold magnification using a color CCD camera (Leica DFC 420C, 5 Mpixels). Subsequently, the embryo size was measured by determining the embryo area employing the imageJ software [111].

4.5. Mass spectrometric analysis of IAA and IAM

Endogenous IAM and IAA contents have been analyzed by liquid chromatography-mass spectrometry following a previously published protocol [24]. In brief, organic compounds have been extracted from 100 mg of imbibed seeds into 1 ml ice-cold potassium phosphate buffer (50 mM, pH 7.0) containing 1% diethyldithiocarbamic acid sodium salt and 50 pmol of $[^2H_5,^{15}N]$-IAM and $[^2H_5]$-IAA as internal standards. The organic phase was transferred into fresh tubes and acidified (pH 2.7) by adding 1 M hydrochloric acid. After the samples were pre-purified using 1 ml HLB columns, the eluates were taken to dryness *in vacuo* and re-dissolved in 45 µl methanol with 0.1% formic acid (v/v). Subsequently, 10 µl of the samples were subjected LC-MS analysis employing an Ultimate3000 RSLC system (Dionex) and a microTOF-Q II mass spectrometer (Bruker Daltonics). In order to determine the analyte contents, the following ion transitions were monitored: IAM, $m/z = 175.2 \rightarrow 130.1$; $[^2H_5,^{15}N]$-IAM, $m/z = 181.2 \rightarrow 135.1$ (retention time, 6.3 min); IAA, $m/z = 176.2 \rightarrow 130.1$; $[^2H_5]$-IAA, $m/z = 181.2 \rightarrow 135.1$ (retention time 8.8 min). To integrate the corresponding peak areas, the extracted ion chromatograms were analyzed using the DataAnalysis software package (Bruker Daltonics).

4.6. Transcriptomics analysis of the ami1/rty double mutant

Total RNA from 100 mg imbibed Arabidopsis wt and *ami1/rty* mutant seeds was extracted using the RNasy Plant Mini Kit (Qiagen) according to the manufacturer's instructions. The quality and quantity of the extracted RNA was tested by absorbance analysis using a Nanodrop® ND-1000 spectrophotometer (ThermoFisher). Additionally, the RNA samples were tested on a Bioanalyzer 2100 (Agilent) by the CNB Genomics Service (Madrid). Library construction and RNA sequencing (SE50) was performed by the Beijing Genomics Institute (BGI) on Illumina HiSeq™ 2000 machines. Basic data analysis, including data filtering, sequence alignment [112], transcript quantification [113], and differential gene expression analysis [114] was also performed by BGI. For each genotype three biological replicates were processed. The resulting *p*-values were adjusted for multiple testing using the Benjamini-Hochberg correction [115]. An adjusted *p*-value (FDR) of < 0.05 and absolute differential expression of *log2FC* ≥ 1 were arbitrarily chosen to select differentially expressed genes.

The functional classification of DEGs was performed using the MapMan v3.6 software [116], paying special attention to DEGs related with transcriptional regulation and development. Furthermore, functional relationships between the DEGs were investigated employing the stringApp v1.3 [117], MCODE v2.0 [118], and EnrichmentMaps v3.3.1 [119] in Cytoscape v3.8.2 [120]. In order to analyse the importance of the nodes in the inferred networks, the nodes with the highest degree of connectivity (k) and betweenness centrality (BC) have been examined in closer detail.

Selected transcripts were validated in independent experiments by qRT-PCR. For this, 7-day-old wt seedlings were incubated for 2 h either in ½ MS or ½ MS with 20 µM IAM. For each condition, total RNA from three independent biological replicates was harvested and analysed in triplicate (technical replicates). First-strand synthesis was performed according to the supplier's instructions, using M-MLV reverse transcriptase and oligo(dT)₁₅ primer (Promega). Two nanograms of cDNA were used as template for the qRT-PCR, which was performed according to the manufacturer's

instructions using the FastStart SYBR Green Master solution (Roche Diagnostics) on a Lightcycler 480 Real-Time PCR system (Roche Diagnostics). Relative quantification of expression was calculated after data analysis by the Lightcycler 480 software (Roche Diagnostics), using the comparative $2^{-\Delta\Delta CT}$ method [121] with *APT1* (At1g27450) as reference gene [122]. See Supplementary Table S2 for primer sequences.

4.7. Statistical analysis

We used JASP v0.14.1 for statistical data assessment and the generation of plots. The box plots display the median, quartiles, and extremes of the compared embryo sizes. One-way ANOVA and Tukey's *post-hoc* test or Student's *t*-test were performed to statistically analysis the data. Sample sizes (n) for each experiment are given in the respective figure legends.

Abbreviations

cDNA	complementary DNA
DEPC	diethyl pyrocarbonate
FDR	false discovery rate
FC	fold-change
qRT-PCR	Quantitative reverse transcriptase polymerase chain reaction
T-DNA	transfer DNA

References

1. Davies, P.J. *Plant hormones. Biosynthesis, Signal Transduction, Action!*, 3 ed.; Springer Netherlands: Dordrecht, Boston, London, 2010; 10.1007/978-1-4020-2686-7pp. XIV, 802.

2. Zhao, Y. Auxin biosynthesis and its role in plant development. *Annu Rev Plant Biol* **2010**, *61*, 49-64, doi:10.1146/annurev-arplant-042809-112308.

3. Stepanova, A.N.; Yun, J.; Robles, L.M.; Novak, O.; He, W.; Guo, H.; Ljung, K.; Alonso, J.M. The *Arabidopsis* YUCCA1 flavin monooxygenase functions in the indole-3-pyruvic acid branch of auxin biosynthesis. *Plant Cell* **2011**, *23*, 3961-3973, doi:10.1105/tpc.111.088047.

4. Won, C.; Shen, X.; Mashiguchi, K.; Zheng, Z.; Dai, X.; Cheng, Y.; Kasahara, H.; Kamiya, Y.; Chory, J.; Zhao, Y. Conversion of tryptophan to indole-3-acetic acid by TRYPTOPHAN AMINOTRANSFERASES OF ARABIDOPSIS and YUCCAs in *Arabidopsis*. *Proc Natl Acad Sci U S A* **2011**, *108*, 18518-18523, doi:10.1073/pnas.1108436108.

5. Ljung, K. Auxin metabolism and homeostasis during plant development. *Development* **2013**, *140*, 943-950, doi:10.1242/dev.086363.

6. Pollmann, S.; Müller, A.; Weiler, E.W. Many roads lead to "auxin": of nitrilases, synthases, and amidases. *Plant Biol (Stuttg)* **2006**, *8*, 326-333, doi:10.1055/s-2006-924075.

7. Kasahara, H. Current aspects of auxin biosynthesis in plants. *Biosci Biotechnol Biochem* **2016**, *80*, 34-42, doi:10.1080/09168451.2015.1086259.

8. Zhao, Y. Auxin biosynthesis. *Arabidopsis Book* **2014**, *12*, e0173, doi:10.1199/tab.0173.

9. Zhao, Y.; Hull, A.K.; Gupta, N.R.; Goss, K.A.; Alonso, J.; Ecker, J.R.; Normanly, J.; Chory, J.; Celenza, J.L. Trp-dependent auxin biosynthesis in *Arabidopsis*: involvement of cytochrome P450s CYP79B2 and CYP79B3. *Genes Dev* **2002**, *16*, 3100-3112, doi:10.1101/gad.1035402.

10. Sugawara, S.; Hishiyama, S.; Jikumaru, Y.; Hanada, A.; Nishimura, T.; Koshiba, T.; Zhao, Y.; Kamiya, Y.; Kasahara, H. Biochemical analyses of indole-3-acetaldoxime-dependent auxin biosynthesis in *Arabidopsis*. *Proc Natl Acad Sci U S A* **2009**, *106*, 5430-5435, doi:10.1073/pnas.0811226106.

11. Glawischnig, E.; Hansen, B.G.; Olsen, C.E.; Halkier, B.A. Camalexin is synthesized from indole-3-acetaldoxime, a key branching point between primary and secondary metabolism in *Arabidopsis*. *Proc Natl Acad Sci U S A* **2004**, *101*, 8245-8250, doi:10.1073/pnas.0305876101.

12. Sønderby, I.E.; Geu-Flores, F.; Halkier, B.A. Biosynthesis of glucosinolates - gene discovery and beyond. *Trends Plant Sci* **2010**, *15*, 283-290, doi:10.1016/j.tplants.2010.02.005.

13. Glawischnig, E. Camalexin. *Phytochemistry* **2007**, *68*, 401-406, doi:10.1016/j.phytochem.2006.12.005.

14. Frerigmann, H.; Gigolashvili, T. MYB34, MYB51, and MYB122 distinctly regulate indolic glucosinolate biosynthesis in *Arabidopsis thaliana*. *Mol Plant* **2014**, *7*, 814-828, doi:10.1093/mp/ssu004.

15. Birkenbihl, R.P.; Diezel, C.; Somssich, I.E. Arabidopsis WRKY33 is a key transcriptional regulator of hormonal and metabolic responses toward *Botrytis cinerea* infection. *Plant Physiol* **2012**, *159*, 266-285, doi:10.1104/pp.111.192641.

16. Lehmann, T.; Janowitz, T.; Sánchez-Parra, B.; Pérez-Alonso, M.M.; Trompetter, I.; Piotrowski, M.; Pollmann, S. *Arabidopsis* NITRILASE 1 Contributes to the Regulation of Root Growth and Development through Modulation of Auxin Biosynthesis in Seedlings. *Front Plant Sci* **2017**, *8*, 36, doi:10.3389/fpls.2017.00036.

17. Frerigmann, H.; Pislewska-Bednarek, M.; Sanchez-Vallet, A.; Molina, A.; Glawischnig, E.; Gigolashvili, T.; Bednarek, P. Regulation of Pathogen-Triggered Tryptophan Metabolism in Arabidopsis thaliana by MYB Transcription Factors and Indole Glucosinolate Conversion Products. *Mol Plant* **2016**, *9*, 682-695, doi:10.1016/j.molp.2016.01.006.

18. Lehmann, T.; Hoffmann, M.; Hentrich, M.; Pollmann, S. Indole-3-acetamide-dependent auxin biosynthesis: a widely distributed way of indole-3-acetic acid production? *Eur J Cell Biol* **2010**, *89*, 895-905, doi:10.1016/j.ejcb.2010.06.021.

19. Klee, H.J.; Horsch, R. B.; Hinchee, M. A. Hein, M. B.; Hoffmann, N. L. The effects of overproduction of two *Agrobacterium tumefaciens* T-DNA auxin biosynthetic gene products in transgenic petunia plants. *Genes Dev* **1987**, *1*, 86-96, doi:10.1101/gad.1.1.86.

20. Gielen, J.; De Beuckeleer, M.; Seurinck, J.; Deboeck, F.; De Greve, H.; Lemmers, M.; Van Montagu, M.; Schell, J. The complete nucleotide sequence of the TL-DNA of the *Agrobacterium tumefaciens* plasmid pTiAch5. *EMBO J* **1984**, *3*, 835-846, doi: 10.1002/j.1460-2075.1984.tb01894.x.

21. Boerjan, W.; Cervera, M.T.; Delarue, M.; Beeckman, T.; Dewitte, W.; Bellini, C.; Caboche, M.; Van Onckelen, H.; Van Montagu, M.; Inzé, D. *superroot*, a recessive mutation in Arabidopsis, confers auxin overproduction. *Plant Cell* **1995**, *7*, 1405-1419, doi:10.1105/tpc.7.9.1405.

22. Delarue, M.; Prinsen, E.; Onckelen, H.V.; Caboche, M.; Bellini, C. *Sur2* mutations of *Arabidopsis thaliana* define a new locus involved in the control of auxin homeostasis. *Plant J* **1998**, *14*, 603-611, doi:10.1046/j.1365-313x.1998.00163.x.

23. King, J.J.; Stimart, D.P.; Fisher, R.H.; Bleecker, A.B. A Mutation Altering Auxin Homeostasis and Plant Morphology in Arabidopsis. *Plant Cell* **1995**, *7*, 2023-2037, doi:10.1105/tpc.7.12.2023.

24. Pérez-Alonso, M.M.; Ortiz-García, P.; Moya-Cuevas, J.; Lehmann, T.; Sánchez-Parra, B.; Björk, R.G.; Karim, S.; Amirjani, M.R.; Aronsson, H.; Wilkinson, M.D., et al. Endogenous indole-3-acetamide levels contribute to the crosstalk between auxin and abscisic acid, and trigger plant stress responses in *Arabidopsis thaliana*. *J Exp Bot* **2020**, ahead of print, doi:10.1093/jxb/eraa485.

25. Tenorio-Berrío, R.; Pérez-Alonso, M.M.; Vicente-Carbajosa, J.; Martín-Torres, L.; Dreyer, I.; Pollmann, S. Identification of Two Auxin-Regulated Potassium Transporters Involved in Seed Maturation. *Int J Mol Sci* **2018**, *19*, doi:10.3390/ijms19072132.

26. Mikkelsen, M.D.; Naur, P.; Halkier, B.A. Arabidopsis mutants in the *C–S* lyase of glucosinolate biosynthesis establish a critical role for indole-3-acetaldoxime in auxin homeostasis. *Plant J* **2004**, *37*, 770-777, doi:10.1111/j.1365-313X.2004.02002.x.

27. Barlier, I.; Kowalczyk, M.; Marchant, A.; Ljung, K.; Bhalerao, R.; Bennett, M.; Sandberg, G.; Bellini, C. The *SUR2* gene of *Arabidopsis thaliana* encodes the cytochrome P450 CYP83B1, a modulator of auxin homeostasis. *Proc Natl Acad Sci U S A* **2000**, *97*, 14819-14824, doi:10.1073/pnas.260502697.

28. Bak, S.; Tax, F.E.; Feldmann, K.A.; Galbraith, D.W.; Feyereisen, R. CYP83B1, a cytochrome P450 at the metabolic branch point in auxin and indole glucosinolate biosynthesis in Arabidopsis. *Plant Cell* **2001**, *13*, 101-111, doi:10.1105/tpc.13.1.101.

29. Brumos, J.; Bobay, B.G.; Clark, C.A.; Alonso, J.M.; Stepanova, A.N. Structure-Function Analysis of Interallelic Complementation in *ROOTY* Transheterozygotes. *Plant Physiol* **2020**, *183*, 1110-1125, doi:10.1104/pp.20.00310.

30. Giustini, C.; Graindorge, M.; Cobessi, D.; Crouzy, S.; Robin, A.; Curien, G.; Matringe, M. Tyrosine metabolism: identification of a key residue in the acquisition of prephenate aminotransferase activity by 1ß aspartate aminotransferase. *FEBS J* **2019**, *286*, 2118-2134, doi:10.1111/febs.14789.

31. Gao, Y.; Dai, X.; Aoi, Y.; Takebayashi, Y.; Yang, L.; Guo, X.; Zeng, Q.; Yu, H.; Kasahara, H.; Zhao, Y. Two homologous *INDOLE-3-ACETAMIDE (IAM) HYDROLASE* genes are required for the auxin effects of IAM in *Arabidopsis*. *J Genet Genom* **2020**, *47*, 157-165, doi:10.1016/j.jgg.2020.02.009.

32. Morant, M.; Ekstrøm, C.; Ulvskov, P.; Kristensen, C.; Rudemo, M.; Olsen, C.E.; Hansen, J.; Jørgensen, K.; Jørgensen, B.; Møller, B.L., et al. Metabolomic, Transcriptional, Hormonal, and Signaling Cross-talk in *superroot2*. *Mol Plant* **2010**, *3*, 192-211, doi:10.1093/mp/ssp098.

33. Molesini, B.; Rotino, G.L.; Spena, A.; Pandolfini, T. Expression profile analysis of early fruit development in *iaaM*-parthenocarpic tomato plants. *BMC Res Notes* **2009**, *2*, 143, doi:10.1186/1756-0500-2-143.

34. Romano, C.P.; Robson, P.R.H.; Smith, H.; Estelle, M.; Klee, H. Transgene-mediated auxin overproduction in *Arabidopsis*: hypocotyl elongation phenotype and interactions with the *hy6-1* hypocotyl elongation and *axr1* auxin-resistant mutants. *Plant Mol Biol* **1995**, *27*, 1071-1083, doi:10.1007/BF00020881.

35.   Mashiguchi, K.; Hisano, H.; Takeda-Kamiya, N.; Takebayashi, Y.; Ariizumi, T.; Gao, Y.; Ezura, H.; Sato, K.; Zhao, Y.; Hayashi, K.-i., et al. *Agrobacterium tumefaciens* Enhances Biosynthesis of Two Distinct Auxins in the Formation of Crown Galls. *Plant Cell Physiol* **2018**, *60*, 29-37, doi:10.1093/pcp/pcy182.

36.   Liu, X.; Zhang, H.; Zhao, Y.; Feng, Z.; Li, Q.; Yang, H.Q.; Luan, S.; Li, J.; He, Z.H. Auxin controls seed dormancy through stimulation of abscisic acid signaling by inducing ARF-mediated *ABI3* activation in *Arabidopsis*. *Proc Natl Acad Sci U S A* **2013**, *110*, 15485-15490, doi:10.1073/pnas.1304651110.

37.   Nitsch, J.P. Growth and morphogenesis of the strawberry as related to auxin. *Am J Bot* **1950**, *37*, 211-215, doi:10.1002/j.1537-2197.1950.tb12183.x.

38.   Estrada-Johnson, E.; Csukasi, F.; Pizarro, C.M.; Vallarino, J.G.; Kiryakova, Y.; Vioque, A.; Brumos, J.; Medina-Escobar, N.; Botella, M.A.; Alonso, J.M., et al. Transcriptomic Analysis in Strawberry Fruits Reveals Active Auxin Biosynthesis and Signaling in the Ripe Receptacle. *Front Plant Sci* **2017**, *8*, 889, doi:10.3389/fpls.2017.00889.

39.   Symons, G.M.; Chua, Y.J.; Ross, J.J.; Quittenden, L.J.; Davies, N.W.; Reid, J.B. Hormonal changes during non-climacteric ripening in strawberry. *J Exp Bot* **2012**, *63*, 4741-4750, doi:10.1093/jxb/ers147.

40.   Rotino, G.L.; Perri, E.; Zottini, M.; Sommer, H.; Spena, A. Genetic engineering of parthenocarpic plants. *Nat Biotechnol* **1997**, *15*, 1398-1401, doi:10.1038/nbt1297-1398.

41.   Acciarri, N.; Restaino, F.; Vitelli, G.; Perrone, D.; Zottini, M.; Pandolfini, T.; Spena, A.; Rotino, G. Genetically modified parthenocarpic eggplants: improved fruit productivity under both greenhouse and open field cultivation. *BMC Biotechnol* **2002**, *2*, 4, doi:10.1186/1472-6750-2-4.

42.   Martinelli, F.; Uratsu, S.L.; Reagan, R.L.; Chen, Y.; Tricoli, D.; Fiehn, O.; Rocke, D.M.; Gasser, C.S.; Dandekar, A.M. Gene regulation in parthenocarpic tomato fruit. *J Exp Bot* **2009**, *60*, 3873-3890, doi:10.1093/jxb/erp227.

43.   White, P.J. Recent advances in fruit development and ripening: an overview. *J Exp Bot* **2002**, *53*, 1995-2000, doi:10.1093/jxb/erf105.

44.   Pabón-Mora, N.; Litt, A. Comparative anatomical and developmental analysis of dry and fleshy fruits of Solanaceae. *Am J Bot* **2011**, *98*, 1415-1436, doi:10.3732/ajb.1100097.

45.   Ballester, P.; Ferrándiz, C. Shattering fruits: variations on a dehiscent theme. *Curr Opin Plant Biol* **2017**, *35*, 68-75, doi:10.1016/j.pbi.2016.11.008.

46.   McAdam, E.L.; Meitzel, T.; Quittenden, L.J.; Davidson, S.E.; Dalmais, M.; Bendahmane, A.I.; Thompson, R.; Smith, J.J.; Nichols, D.S.; Urquhart, S., et al. Evidence that auxin is required for normal seed size and starch synthesis in pea. *New Phytol* **2017**, *216*, 193-204, doi: 10.1111/nph.14690.

47.   Brown, R.C.; Lemmon, B.E.; Nguyen, H.; Olsen, O.-A. Development of endosperm in *Arabidopsis thaliana*. *Sex Plant Reprod* **1999**, *12*, 32-42, doi:10.1007/s004970050169.

48.   Hentrich, M.; Böttcher, C.; Düchting, P.; Cheng, Y.; Zhao, Y.; Berkowitz, O.; Masle, J.; Medina, J.; Pollmann, S. The jasmonic acid signaling pathway is linked to auxin homeostasis through the modulation of *YUCCA8* and *YUCCA9* gene expression. *Plant J* **2013**, *74*, 626-637, doi:10.1111/tpj.12152.

49.   Gopalraj, M.; Tseng, T.-S.; Olszewski, N. The *Rooty* gene of *Arabidopsis* encodes a protein with highest similarity to aminotransferases. *Plant Physiol* **1996**, *111*, S-114.

50.   Mackelprang, R.; Okrent, R.A.; Wildermuth, M.C. Preference of *Arabidopsis thaliana* GH3.5 acyl amido synthetase for growth versus defense hormone acyl substrates is dictated by concentration of amino acid substrate aspartate. *Phytochemistry* **2017**, *143*, 19-28, doi:10.1016/j.phytochem.2017.07.001.

51.   Jackson, R.G.; Lim, E.-K.; Li, Y.; Kowalczyk, M.; Sandberg, G.; Hoggett, J.; Ashford, D.A.; Bowles, D.J. Identification and Biochemical Characterization of an *Arabidopsis* Indole-3-acetic Acid Glucosyltransferase. *J Biol Chem* **2001**, *276*, 4350-4356, doi:10.1074/jbc.M006185200.

52.   Ludwig-Müller, J. Indole-3-butyric acid synthesis in ecotypes and mutants of *Arabidopsis thaliana* under different growth conditions. *J Plant Physiol* **2007**, *164*, 47-59, doi:10.1016/j.jplph.2005.10.008.

53.   Meßner, B.; Thulke, O.; Schäffner, A.R. *Arabidopsis* glucosyltransferases with activities toward both endogenous and xenobiotic substrates. *Planta* **2003**, *217*, 138-146, doi:10.1007/s00425-002-0969-0.

54.   Hamann, T.; Mayer, U.; Jürgens, G. The auxin-insensitive bodenlos mutation affects primary root formation and apical-basal patterning in the *Arabidopsis* embryo. *Development* **1999**, *126*, 1387-1395.

55.   Hamann, T.; Benkova, E.; Bäurle, I.; Kientz, M.; Jürgens, G. The A*rabidopsis BODENLOS* gene encodes an auxin response protein inhibiting MONOPTEROS-mediated embryo patterning. *Genes Dev* **2002**, *16*, 1610-1615, doi:10.1101/gad.229402.

56.   Weijers, D.; Benkova, E.; Jäger, K.E.; Schlereth, A.; Hamann, T.; Kientz, M.; Wilmoth, J.C.; Reed, J.W.; Jürgens, G. Developmental specificity of auxin response by pairs of ARF and Aux/IAA transcriptional regulators. *EMBO J* **2005**, *24*, 1874-1885, doi:10.1038/sj.emboj.7600659.

57.   Tsuchimatsu, T.; Kakui, H.; Yamazaki, M.; Marona, C.; Tsutsui, H.; Hedhly, A.; Meng, D.; Sato, Y.; Städler, T.; Grossniklaus, U., et al. Adaptive reduction of male gamete number in the selfing plant *Arabidopsis thaliana*. *Nat Commun* **2020**, *11*, 2885, doi:10.1038/s41467-020-16679-7.

58.   Rakitina, D.V.; Taliansky, M.; Brown, J.W.S.; Kalinina, N.O. Two RNA-binding sites in plant fibrillarin provide interactions with various RNA substrates. *Nucleic Acids Res* **2011**, *39*, 8869-8880, doi:10.1093/nar/gkr594.

59.   Li, R.; Sun, R.; Hicks, G.R.; Raikhel, N.V. *Arabidopsis* ribosomal proteins control vacuole trafficking and developmental programs through the regulation of lipid metabolism. *Proc Natl Acad Sci U S A* **2015**, *112*, E89-E98, doi:10.1073/pnas.1422656112.

60.   Kanehisa, M.; Goto, S. KEGG: Kyoto Encyclopedia of Genes and Genomes. *Nucleic Acids Res* **2000**, *28*, 27-30, doi:10.1093/nar/28.1.27.

61.   Mohn, M.A.; Thaqi, B.; Fischer-Schrader, K. Isoform-Specific NO Synthesis by *Arabidopsis thaliana* Nitrate Reductase. *Plants (Basel)* **2019**, *8*, doi:10.3390/plants8030067.

62.   Ashburner, M.; Ball, C.A.; Blake, J.A.; Botstein, D.; Butler, H.; Cherry, J.M.; Davis, A.P.; Dolinski, K.; Dwight, S.S.; Eppig, J.T., et al. Gene ontology: tool for the unification of biology. The Gene Ontology Consortium. *Nat Genet* **2000**, *25*, 25-29, doi:10.1038/75556.

63.   Bray, E.A. Genes commonly regulated by water-deficit stress in *Arabidopsis thaliana*. *J Exp Bot* **2004**, *55*, 2331-2341, doi:10.1093/jxb/erh270.

64.   Barajas-Lopez, J.d.D.; Tiwari, A.; Zarza, X.; Shaw, M.W.; Pascual, J.; Punkkinen, M.; Bakowska, J.C.; Munnik, T.; Fujii, H. EARLY RESPONSE TO DEHYDRATION 7 Remodels Cell Membrane Lipid Composition during Cold Stress in Arabidopsis. *Plant Cell Physiol* **2020**, 10.1093/pcp/pcaa139, doi:10.1093/pcp/pcaa139.

65.   Mittler, R.; Kim, Y.; Song, L.; Coutu, J.; Coutu, A.; Ciftci-Yilmaz, S.; Lee, H.; Stevenson, B.; Zhu, J.-K. Gain- and loss-of-function mutations in *Zat10* enhance the tolerance of plants to abiotic stress. *FEBS Lett* **2006**, *580*, 6537-6542, doi:10.1016/j.febslet.2006.11.002.

66.   Taji, T.; Ohsumi, C.; Iuchi, S.; Seki, M.; Kasuga, M.; Kobayashi, M.; Yamaguchi-Shinozaki, K.; Shinozaki, K. Important roles of drought- and cold-inducible genes for galactinol synthase in stress tolerance in *Arabidopsis thaliana*. *Plant J* **2002**, *29*, 417-426, doi:10.1046/j.0960-7412.2001.01227.x.

67.   To, A.; Valon, C.; Savino, G.; Guilleminot, J.; Devic, M.; Giraudat, J.; Parcy, F. A Network of Local and Redundant Gene Regulation Governs *Arabidopsis* Seed Maturation. *Plant Cell* **2006**, *18*, 1642-1651, doi:10.1105/tpc.105.039925.

68.   Smolikova, G.; Leonova, T.; Vashurina, N.; Frolov, A.; Medvedev, S. Desiccation Tolerance as the Basis of Long-Term Seed Viability. *Int J Mol Sci* **2020**, *22*, doi:10.3390/ijms22010101.

69.   Panikashvili, D.; Shi, J.X.; Bocobza, S.; Franke, R.B.; Schreiber, L.; Aharoni, A. The *Arabidopsis* DSO/ABCG11 Transporter Affects Cutin Metabolism in Reproductive Organs and Suberin in Roots. *Mol Plant* **2010**, *3*, 563-575, doi:10.1093/mp/ssp103.

70.   Bjerkan, K.N.; Jung-Roméo, S.; Jürgens, G.; Genschik, P.; Grini, P.E. *Arabidopsis* WD REPEAT DOMAIN55 Interacts with DNA DAMAGED BINDING PROTEIN1 and Is Required for Apical Patterning in the Embryo. *Plant Cell* **2012**, *24*, 1013-1033, doi:10.1105/tpc.111.089425.

71.   Guo, J.; Hu, Y.; Zhou, Y.; Zhu, Z.; Sun, Y.; Li, J.; Wu, R.; Miao, Y.; Sun, X. Profiling of the Receptor for Activated C Kinase 1a (RACK1a) interaction network in *Arabidopsis thaliana*. *Biochem Biophys Res Commun* **2019**, *520*, 366-372, doi:10.1016/j.bbrc.2019.09.142.

72.   Meinke, D.W. Genome-wide identification of *EMBRYO-DEFECTIVE* (*EMB*) genes required for growth and development in Arabidopsis. *New Phytol* **2020**, *226*, 306-325, doi:10.1111/nph.16071.

73.   Dill, A.; Thomas, S.G.; Hu, J.; Steber, C.M.; Sun, T.-p. The Arabidopsis F-Box Protein SLEEPY1 Targets Gibberellin Signaling Repressors for Gibberellin-Induced Degradation. *Plant Cell* **2004**, *16*, 1392-1405, doi:10.1105/tpc.020958.

74.   Wang, X.-C.; Wu, J.; Guan, M.-L.; Zhao, C.-H.; Geng, P.; Zhao, Q. *Arabidopsis* MYB4 plays dual roles in flavonoid biosynthesis. *Plant J* **2020**, *101*, 637-652, doi:10.1111/tpj.14570.

75.   Mitra, M.; Agarwal, P.; Roy, S. The N-terminal MYB domains affect the stability and folding aspects of *Arabidopsis thaliana* MYB4 transcription factor under thermal stress. *Protoplasma* **2021**, ahead of print, doi:10.1007/s00709-020-01590-1.

76.   Ciftci-Yilmaz, S.; Morsy, M.R.; Song, L.; Coutu, A.; Krizek, B.A.; Lewis, M.W.; Warren, D.; Cushman, J.; Connolly, E.L.; Mittler, R. The EAR-motif of the Cys2/His2-type zinc finger protein Zat7 plays a key role in the defense response of *Arabidopsis* to salinity stress. *J Biol Chem* **2007**, *282*, 9260-9268, doi:10.1074/jbc.M611093200.

77.   Liu, X.-M.; An, J.; Han, H.J.; Kim, S.H.; Lim, C.O.; Yun, D.-J.; Chung, W.S. ZAT11, a zinc finger transcription factor, is a negative regulator of nickel ion tolerance in Arabidopsis. *Plant Cell Rep* **2014**, *33*, 2015-2021, doi:10.1007/s00299-014-1675-7.

78.   Schön, M.; Töller, A.; Diezel, C.; Roth, C.; Westphal, L.; Wiermer, M.; Somssich, I.E. Analyses of *wrky18 wrky40* Plants Reveal Critical Roles of SA/EDS1 Signaling and Indole-Glucosinolate Biosynthesis for *Golovinomyces orontii* Resistance and a Loss-of Resistance Towards *Pseudomonas syringae* pv. tomato AvrRPS4. *Mol Plant Microbe Interact* **2013**, *26*, 758-767, doi:10.1094/mpmi-11-12-0265-r.

79.   Xu, X.; Chen, C.; Fan, B.; Chen, Z. Physical and Functional Interactions between Pathogen-Induced *Arabidopsis* WRKY18, WRKY40, and WRKY60 Transcription Factors. *Plant Cell* **2006**, *18*, 1310-1326, doi:10.1105/tpc.105.037523.

80.   Ahmad, R.; Liu, Y.; Wang, T.-J.; Meng, Q.; Yin, H.; Wang, X.; Wu, Y.; Nan, N.; Liu, B.; Xu, Z.-Y. GOLDEN2-LIKE Transcription Factors Regulate *WRKY40* Expression in Response to Abscisic Acid. *Plant Physiol* **2019**, *179*, 1844-1860, doi:10.1104/pp.18.01466.

81.   Charng, Y.-y.; Liu, H.-c.; Liu, N.-y.; Chi, W.-t.; Wang, C.-n.; Chang, S.-h.; Wang, T.-t. A Heat-Inducible Transcription Factor, HsfA2, Is Required for Extension of Acquired Thermotolerance in *Arabidopsis*. *Plant Physiol* **2007**, *143*, 251-262, doi:10.1104/pp.106.091322.

82.   Song, C.C., Woo Sik ; Lim, C.O. Overexpression of Heat Shock Factor Gene *HsfA3* Increases Galactinol Levels and Oxidative Stress Tolerance in *Arabidopsis*. *Mol. Cells* **2016**, *39*, 477-483, doi:10.14348/molcells.2016.0027.

83.   Jeon, J.; Cho, C.; Lee, M.R.; Van Binh, N.; Kim, J. *CYTOKININ RESPONSE FACTOR2*   (*CRF2*) and *CRF3* Regulate Lateral Root Development in Response to Cold Stress in Arabidopsis. *Plant Cell* **2016**, *28*, 1828-1843, doi:10.1105/tpc.15.00909.

84.   Zwack, P.J.; Compton, M.A.; Adams, C.I.; Rashotte, A.M. Cytokinin response factor 4 (CRF4) is induced by cold and involved in freezing tolerance. *Plant Cell Rep* **2016**, *35*, 573-584, doi:10.1007/s00299-015-1904-8.

85.   Balsemão-Pires, E.; Andrade, L.R.; Sachetto-Martins, G. Functional study of TCP23 in *Arabidopsis thaliana* during plant development. *Plant Physiol Biochem* **2013**, *67*, 120-125, doi:10.1016/j.plaphy.2013.03.009.

86.   Koyama, T.; Furutani, M.; Tasaka, M.; Ohme-Takagi, M. TCP Transcription Factors Control the Morphology of Shoot Lateral Organs via Negative Regulation of the Expression of Boundary-Specific Genes in *Arabidopsis*. *Plant Cell* **2007**, *19*, 473-484, doi:10.1105/tpc.106.044792.

87.   Challa, K.R.; Aggarwal, P.; Nath, U. Activation of *YUCCA5* by the Transcription Factor TCP4 Integrates Developmental and Environmental Signals to Promote Hypocotyl Elongation in Arabidopsis. *Plant Cell* **2016**, *28*, 2117-2130, doi:10.1105/tpc.16.00360.

88.   Qin, G.; Gu, H.; Zhao, Y.; Ma, Z.; Shi, G.; Yang, Y.; Pichersky, E.; Chen, H.; Liu, M.; Chen, Z., et al. An Indole-3-Acetic Acid Carboxyl Methyltransferase Regulates *Arabidopsis* Leaf Development. *Plant Cell* **2005**, *17*, 2693-2704, doi:10.1105/tpc.105.034959.

89.   Richter, R.; Behringer, C.; Müller, I.K.; Schwechheimer, C. The GATA-type transcription factors GNC and GNL/CGA1 repress gibberellin signaling downstream from DELLA proteins and PHYTOCHROME-INTERACTING FACTORS. *Genes Dev* **2010**, *24*, 2093-2104, doi:10.1101/gad.594910.

90.   Beltramino, M.; Ercoli, M.F.; Debernardi, J.M.; Goldy, C.; Rojas, A.M.L.; Nota, F.; Alvarez, M.E.; Vercruyssen, L.; Inzé, D.; Palatnik, J.F., et al. Robust increase of leaf size by *Arabidopsis thaliana* GRF3-like transcription factors under different growth conditions. *Sci Rep* **2018**, *8*, 13447, doi:10.1038/s41598-018-29859-9.

91.   Horiguchi, G.; Kim, G.-T.; Tsukaya, H. The transcription factor AtGRF5 and the transcription coactivator AN3 regulate cell proliferation in leaf primordia of *Arabidopsis thaliana*. *Plant J* **2005**, *43*, 68-78, doi:10.1111/j.1365-313X.2005.02429.x.

92.   Jenik, P.D.; Barton, M.K. Surge and destroy: the role of auxin in plant embryogenesis. *Development* **2005**, *132*, 3577-3585, doi:10.1242/dev.01952.

93.   Möller, B.; Weijers, D. Auxin Control of Embryo Patterning. *Cold Spring Harbor Perspect Biol* **2009**, *1*, doi:10.1101/cshperspect.a001545.

94.   Figueiredo, D.D.; Batista, R.A.; Roszak, P.J.; Hennig, L.; Köhler, C. Auxin production in the endosperm drives seed coat development in *Arabidopsis*. *eLife* **2016**, *5*, e20542, doi:10.7554/eLife.20542.

95.   Abu-Zaitoon, Y.M.; Bennett, K.; Normanly, J.; Nonhebel, H.M. A large increase in IAA during development of rice grains correlates with the expression of tryptophan aminotransferase *OsTAR1* and a grain-specific *YUCCA*. *Physiol Plant* **2012**, *146*, 487-499, doi:10.1111/j.1399-3054.2012.01649.x.

96.   Le Clere , S.; Schmelz, E.A.; Chourey, P.S. Sugar levels regulate tryptophan-dependent auxin biosynthesis in developing maize kernels. *Plant Physiol* **2010**, *153*, 306-318, doi:10.1104/pp.110.155226.

97.   Sairanen, I.; Novák, O.; Pěnčík, A.; Ikeda, Y.; Jones, B.; Sandberg, G.; Ljung, K. Soluble carbohydrates regulate auxin biosynthesis via PIF proteins in *Arabidopsis*. *Plant Cell* **2012**, *24*, 4907-4916, doi:10.1105/tpc.112.104794.

98.   Belda-Palazón, B.; Adamo, M.; Valerio, C.; Ferreira, L.J.; Confraria, A.; Reis-Barata, D.; Rodrigues, A.; Meyer, C.; Rodriguez, P.L.; Baena-González, E. A dual function of SnRK2 kinases in the regulation of SnRK1 and plant growth. *Nature Plants* **2020**, *6*, 1345-1353, doi:10.1038/s41477-020-00778-w.

99.   Emenecker, R.J.; Strader, L.C. Auxin-Abscisic Acid Interactions in Plant Growth and Development. *Biomolecules* **2020**, *10*, doi:10.3390/biom10020281.

100.   Hentrich, M.; Sánchez-Parra, B.; Pérez Alonso, M.M.; Carrasco Loba, V.; Carrillo, L.; Vicente-Carbajosa, J.; Medina, J.; Pollmann, S. *YUCCA8* and *YUCCA9* overexpression reveals a link between auxin signaling and lignification through the induction of ethylene biosynthesis. *Plant Signal Behav* **2013**, *8*, e26363, doi:10.4161/psb.26363.

101.   Aziz, M.; Chapman, K.D. Fatty Acid Amide Hydrolases: An Expanded Capacity for Chemical Communication? *Trends Plant Sci* **2020**, *25*, 236-249, doi:10.1016/j.tplants.2019.11.002.

102.   Shrestha, R.; Dixon, R.A.; Chapman, K.D. Molecular identification of a functional homologue of the mammalian fatty acid amide hydrolase in *Arabidopsis thaliana*. *J Biol Chem* **2003**, *278*, 34990-34997, doi:10.1074/jbc.M305613200.

103.   Klepikova, A.V.; Kasianov, A.S.; Gerasimov, E.S.; Logacheva, M.D.; Penin, A.A. A high resolution map of the *Arabidopsis thaliana* developmental transcriptome based on RNA-seq profiling. *Plant J* **2016**, *88*, 1058-1070, doi:10.1111/tpj.13312.

104.   Micol-Ponce, R.; Sarmiento-Mañús, R.; Fontcuberta-Cervera, S.; Cabezas-Fuster, A.; de Bures, A.; Sáez-Vásquez, J.; Ponce, M.R. SMALL ORGAN4 Is a Ribosome Biogenesis Factor Involved in 5.8S Ribosomal RNA Maturation. *Plant Physiol* **2020**, *184*, 2022-2039, doi:10.1104/pp.19.01540.

105.   Sánchez-García, A.B.; Aguilera, V.; Micol-Ponce, R.; Jover-Gil, S.; Ponce, M.R. Arabidopsis *MAS2*, an Essential Gene That Encodes a Homolog of Animal NF-kappa B Activating Protein, Is Involved in 45S Ribosomal DNA Silencing. *Plant Cell* **2015**, *27*, 1999-2015, doi:10.1105/tpc.15.00135.

106.   Cheng, Y.; Dai, X.; Zhao, Y. Auxin biosynthesis by the YUCCA flavin monooxygenases controls the formation of floral organs and vascular tissues in *Arabidopsis*. *Genes Devel* **2006**, *20*, 1790-1799, doi:10.1101/gad.1415106.

107.   Murashige, T.; Skoog, F. A revised medium for rapid growth and bio assays with tobacco tissue cultures. *Physiol Plant* **1962**, *15*, 473-497.

108.   Alonso, J.M.; Stepanova, A.N.; Leisse, T.J.; Kim, C.J.; Chen, H.; Shinn, P.; Stevenson, D.K.; Zimmerman, J.; Barajas, P.; Cheuk, R., et al. Genome-wide insertional mutagenesis of *Arabidopsis thaliana*. *Science* **2003**, *301*, 653-657, doi:10.1126/science.1086391.

109.   Oñate-Sánchez, L.; Vicente-Carbajosa, J. DNA-free RNA isolation protocols for *Arabidopsis thaliana*, including seeds and siliques. *BMC Res Notes* **2008**, *1*, 93, doi:10.1186/1756-0500-1-93.

110.   Waterhouse, A.; Bertoni, M.; Bienert, S.; Studer, G.; Tauriello, G.; Gumienny, R.; Heer, F.T.; de Beer, T.A P.; Rempfer, C.; Bordoli, L., et al. SWISS-MODEL: homology modelling of protein structures and complexes. *Nucleic Acids Res* **2018**, *46*, W296-W303, doi:10.1093/nar/gky427.

111. Schindelin, J.; Arganda-Carreras, I.; Frise, E.; Kaynig, V.; Longair, M.; Pietzsch, T.; Preibisch, S.; Rueden, C.; Saalfeld, S.; Schmid, B., et al. Fiji: an open-source platform for biological-image analysis. *Nat Methods* **2012**, *9*, 676-682, doi:10.1038/nmeth.2019.

112. Trapnell, C.; Pachter, L.; Salzberg, S.L. TopHat: discovering splice junctions with RNA-Seq. *Bioinformatics* **2009**, *25*, 1105-1111, doi:10.1093/bioinformatics/btp120.

113. Anders, S.; Pyl, P.T.; Huber, W. HTSeq—a Python framework to work with high-throughput sequencing data. *Bioinformatics* **2014**, *31*, 166-169, doi:10.1093/bioinformatics/btu638.

114. Trapnell, C.; Roberts, A.; Goff, L.; Pertea, G.; Kim, D.; Kelley, D.R.; Pimentel, H.; Salzberg, S.L.; Rinn, J.L.; Pachter, L. Differential gene and transcript expression analysis of RNA-seq experiments with TopHat and Cufflinks. *Nat Protoc* **2012**, *7*, 562-578, doi:10.1038/nprot.2012.016.

115. Benjamini, Y.; Hochberg, Y. Controlling the False Discovery Rate: A Practical and Powerful Approach to Multiple Testing. *J Royal Stat Society: B* **1995**, *57*, 289-300, doi:10.1111/j.2517-6161.1995.tb02031.x.

116. Thimm, O.; Bläsing, O.; Gibon, Y.; Nagel, A.; Meyer, S.; Krüger, P.; Selbig, J.; Müller, L.A.; Rhee, S.Y.; Stitt, M. MAPMAN: a user-driven tool to display genomics data sets onto diagrams of metabolic pathways and other biological processes. *Plant J* **2004**, *37*, 914-939, doi:10.1111/j.1365-313X.2004.02016.x.

117. Doncheva, N.T.; Morris, J.H.; Gorodkin, J.; Jensen, L.J. Cytoscape StringApp: Network Analysis and Visualization of Proteomics Data. *J Proteome Res* **2019**, *18*, 623-632, doi:10.1021/acs.jproteome.8b00702.

118. Bader, G.D.; Hogue, C.W.V. An automated method for finding molecular complexes in large protein interaction networks. *BMC Bioinformatics* **2003**, *4*, 2, doi:10.1186/1471-2105-4-2.

119. Merico, D.; Isserlin, R.; Stueker, O.; Emili, A.; Bader, G.D. Enrichment Map: A Network-Based Method for Gene Set Enrichment Visualization and Interpretation. *PLOS ONE* **2010**, *5*, e13984, doi:10.1371/journal.pone.0013984.

120. Shannon, P.; Markiel, A.; Ozier, O.; Baliga, N.S.; Wang, J.T.; Ramage, D.; Amin, N.; Schwikowski, B.; Ideker, T. Cytoscape: A Software Environment for Integrated Models of Biomolecular Interaction Networks. *Genome Res* **2003**, *13*, 2498-2504, doi:10.1101/gr.1239303.

121. Livak, K.J.; Schmittgen, T.D. Analysis of relative gene expression data using real-time quantitative PCR and the 2(-Delta Delta C(T)) Method. *Methods* **2001**, *25*, 402-408, doi:10.1006/meth.2001.1262.

122. Czechowski, T.; Stitt, M.; Altmann, T.; Udvardi, M.K.; Scheible, W.R. Genome-wide identification and testing of superior reference genes for transcript normalization in Arabidopsis. *Plant Physiol* **2005**, *139*, 5-17, doi:10.1104/pp.105.063743.